NASA Contractor Report 141439

The Prediction and Mapping of Geoidal Undulations from GEOS-3 Altimetry

William Kearsley

(NASA-CR-141439) THE PREDICTION AND MAPPING OF GEOIDAL UNDULATIONS FROM GEOS-3 ALTIMETRY (Ohio State Univ. Research Foundation) 52 p HC A04/MF A01 CSCL 08B

N78-25507

Unclas

G3/43 16685

April 1978

National Aeronautics and Space Administration

Wallops Flight Center
Wallops Island, Virginia 23337
AC 804 824-3411

NASA Contractor Report 141439

The Prediction and Mapping of Geoidal Undulations from GEOS-3 Altimetry

William Kearsley
The Ohio State University
Research Foundation
Columbus, Ohio 43212

Prepared Under Contract No. NAS6-2484

NASA
National Aeronautics and
Space Administration

Wallops Flight Center
Wallops Island, Virginia 23337
AC 804 824-3411

Foreword

This report was prepared by Dr. William Kearsley, Research Associate, Department of Geodetic Science, The Ohio State University, under NASA Contract No. NAS 6-2484, The Ohio State University Research Foundation Project No. 783904, Project Supervisor, Richard H. Rapp. The contract covering this research is administered through the NASA Wallops Flight Center, Wallops Island, Virginia 23337, with Mr. Ray Stanley, Project Scientist.

Table of Contents

Acknowledgements

I am indebted to Professor Richard H. Rapp for the opportunity to work with him in the analysis of the GEOS-3 data, and also for his help and encouragement on this project. I would also like to thank Laura Reiter for her care and patience in typing the manuscript of this report.

1. Introduction

This paper is written to describe the methods developed at the Department of Geodetic Science to produce 'geoid' maps over ocean areas using the adjusted altimetry data described in Rapp (1977). This data represents the results of bias and trend removal from the original, but edited, Geos-3 altimeter data supplied by NASA through the Wallops Flight Center.

1.1 Map Specifications

The data forming the basis of the contour maps is the estimated geometric sea surface height ($\bar{h}$) which contains corrections for tropospheric refraction and altitude bias. This provides an estimate of the separation between the sea surface and the adopted reference ellipsoid. If the effects of ocean tides can now be removed from $\bar{h}$, and medium and short wavelength noise filtered, the result will be an estimate of the geoid-spheroid separation, N. To find the best contour interval to adopt for a contour map of the geoid, one must first estimate the error likely to be present in N (δN).

The standard deviations of the adjusted altimeter data are due to instrumental effects and the unmodeled orthometric height, and are estimated to be about ± 1 m for short pulse and ± 2 m for long pulse measurements (Rummel, 1976, p. 12-13). These accuracies can be used to determine a suitable contour interval for geoidal maps based on the altimeter data. For example, the contour interval is usually 3.33 δN (American standards to 5 δN (European standards), δN being the error in individual heights (Richardus, 1973, p. 83), suggesting a contour interval of 3 m to 5 m for data measured in the short pulse mode. However, these standards are for medium to large scale maps. Generally, the geoid is smooth and geoid maps are small scale (e.g. 1:500,000), so it appears reasonable to adopt a 2 m contour interval in this case. This compares well with (Ibid., p. 106) where 2 δN appears to be sufficient contour interval in flat areas.

1.2 Description of Programs

The programs used in the prediction and contouring of the undulations are referred to throughout the report and are listed here with a brief description for convenience. They were written for the IBM 370 at the Ohio State University, which is equipped with an on-line VERSATEC plotter. The details for user operation are given in Appendix A, and a Flow Chart of the program MAIN can be found in Appendix B.

Programs used in the production version of the contouring package include:

(i) MAIN which reads all altimetry data from the relevant tape, and having passed this data through a window specifying the map limits, organizes the subroutine used to predict geoid values, plot the contours and axes, and so on. (See Appendix B for Flow Chart)

(ii) GPP the general plotting package developed by the Computer Services Unit to facilitate plotting on the VERSATEC plotter.

(iii) PRDT a subroutine originally developed by Snowden (1969), but largely rewritten to suit the present task and system more closely.

(iv) GEOGRD a subroutine to convert geographical to projection coordinates using a spherical model of the earth of radius 6.371×10^6 m. Options include the Plate-Carrée, Mercator, Cassini-Soldner and Equal Area Conical and Cylindrical projections (see also Pearson, 1977).

(v) COVA a subroutine to compute global or local covariance functions (Tscherning and Rapp, 1973).

(vi) CGTOUR a subroutine developed by Snowden (1969) which plots and annotates contours from gridded data.

(vii) AXPLT a subroutine developed to plot and annotate rectangular map borders.

(viii) SHLN a subroutine developed to plot the coastlines of those land masses falling within the mapping limits.

2. Filtering the Altimetry Data

The data to be used in this report has been processed to minimize the large long wavelength and constant biases in the original data. The information which is now relevant to the contouring process is (i) the measurement type, (ii) the sequence number, (iii) geocentric latitude, (iv) geocentric longitude, (v) the estimated standard deviation of the range and (vi) the adjusted sea surface height (for these purposes, equivalent to the geoid height, N).

The adjusted data contains high-frequency noise which should be filtered before it is used in production (Rummel, 1976, pp. 12-15). A least-squares filtering technique developed by Rummel was used for this purpose. Using a band width of 11 points the filter is passed through each segment of an orbit, such that data from any adjacent segment is not used in the filtering process.

Table 1 shows typical filters developed for an 11 point band width. Filter No. 1 is applied when the subject data is the first in the 11 point section, Filter No. 6 where the subject data is the sixth, and so on in reverse order (e.g. Filter 5 for point 7). The filter values are generated from subroutine COVA (Section 1.3) based on the lag of the data points averaged over the segment for test purposes.

The data for the Alaska test area, which resulted from a preliminary adjustment, was also passed through a filter using a moving averages technique and the results compared with those from the least-squares method. Using a sample of about 400 points it showed that 85% of the values from the moving averages method differed by less than 0.1 m, and 95% differed by less than 0.15 m. The largest differences (0.25) occurred at the terminals of the sections. This suggests that the moving-averages method introduces no significant error (cf. the least squares approach) in data being used to plot 2 m contours (see Section 1.2), and costs about 2/3 the cost of the former approach.

Table 1

Coefficients of Typical Filters Generated from COVA
for Least Squares Filtering

Filter #	Filter Values										
1	0.24	0.20	0.16	0.13	0.10	0.07	0.05	0.03	0.01	0.00	-0.02
2	0.20	0.18	0.16	0.13	0.10	0.08	0.06	0.04	0.02	0.01	0.00
3	0.16	0.16	0.15	0.13	0.11	0.09	0.07	0.05	0.04	0.02	0.01
4	0.13	0.13	0.13	0.13	0.11	0.10	0.08	0.06	0.05	0.04	0.03
5	0.10	0.10	0.11	0.11	0.12	0.11	0.09	0.08	0.07	0.06	0.05
6	0.07	0.08	0.09	0.10	0.11	0.11	0.11	0.10	0.09	0.08	0.07

A question arises which concerns the order in which the adjustment and the filtering is performed. The long wavelength errors ($n < 20$, where n denotes the degree of a Legendre polynomial expansion between $-\pi$ and $+\pi$) result from errors in the computed orbits. The medium ($20 \leq n \leq 200$) and short ($n > 200$) wavelength errors are due mainly to sea surface state and altimeter noise. In theory one should remove these errors before the external constrains at crossover points are placed on the data during the adjustment. In practice, it was found too expensive to filter the data, and the need for such a filter was diminished by the fact that (i) the data had already been passed through a coarse filter (Rapp, 1977, pp. 1, 2) and (ii) the process of predicting the grid point value itself performs a smoothing or filtering function.

As a result, all maps produced once tests had been completed and the program finalized (i.e. Figures 6 - 45) used adjusted data which had not been filtered.

3. Interpolation of Data for Contouring

3.1 Least Squares Prediction

The method of observation results in the data being densely spaced along the satellite track (0.3 degree), with the spacing between tracks in the test area being comparatively large and irregular. Attempts to contour direct from the data failed, and it was necessary to interpolate the data onto a grid pattern in order to take advantage of the subroutine CGTOUR developed by Snowden (1969).

The subroutine PRDT was developed for this purpose. This generates a grid, the dimensions of which are specified by the user and then, using a least squares prediction technique, estimates a value for the geoid height at each of the grid points. An estimate of accuracy is also given for this value. This information can now be used by subroutine CGTOUR to obtain and plot geoidal contours for the area.

A note should be made here concerning the accuracy estimates. These will be based on (i) the standard deviation of the data used in the prediction and (ii) the separation of these data points from the prediction (grid) point. The standard deviations in (i) are supplied with the original data and are a measure of internal consistency (rather than of absolute accuracy) of the repeated observations used to obtain the mean altimeter range value. The prediction error in (ii) is a test of how well the data fits the statistical model assumed in the least squares prediction. The accuracies computed can not therefore claim to be absolute but are a good indication of the precision or relative accuracies of the predicted values. The value of having this information can be appreciated by referring to Figure 2, where one can clearly see how the errors are related to the tracks of the satellite orbits (and hence the separation between the prediction and data points). For comments relating to the accuracy of the contour map, see Section 4. The results of the predictions and their errors along with their respective plots, for a 15° x 10° region in the Alaska test area, are shown in Tables 2 and 3 and Figures 1 and 2.

The basis of the least squares prediction is the covariance function which expresses the covariance relationships between any two geoid undulation values. The subroutine COVA (Tscherning and Rapp, 1975) was used to generate these covariance values. Attempts were made to simplify and speed up the computation by using simple polynomial models such as the second and third order Markov models suggested by Jordan (1972), and the Gaussian model by Moritz (1972), but the time saving was negligible and in some cases, the predicted values were obviously wrong. For example, in one instance the value differed by about 300 m from that predicted by COVA. This erratic behavior was caused by instability of the auto-covariance matrix generated by the third-order Markov function, which is uncritical for small changes in ψ as $\psi \to 0$. The second-order Markov function is more sensitive in this region and was found preferable in practical computation, even though it is felt to be a poorer reflection of the true behavior of the covariance function for small ψ (Jordan, 1972).

Another alternative has been suggested by Lachapelle (1976, p. 7), who found a saving of a factor of 2.5 to 3 when a tabulation of covariance values generated from COVA was used. When this was adopted, some saving was noted, although not nearly as dramatic as that mentioned above. The apparent reason for this is that only the total cost of the program is known, and part of it-that of contouring the gridded geoid height and accuracy values-remains constant and fairly expensive. The final version of the program uses a tabulation of COVA values at every 0.05 degrees, $0 \le \psi \le 10$, and employs a linear interpolation to extract $C(\psi)$ when ψ is not an even 0°.05 value.

3.2 Prediction by Weighted Means

The simple deterministic model:

$$\hat{N}_j = \frac{\sum_{i=1}^{n} N_i / r_{ij}^{\nu}}{\sum_{i=1}^{n} 1 / r_{ij}^{\nu}}$$

where

$\hat{N}_j$ = predicted value of N at point j
N_i = value of N at point i
r_{ij} = separation between points i and j
ν = power of prediction
and n = number of observations

has been used by Sjöberg (1975, p. 7) to predict gravity anomalies (also see Davis, 1973, pp. 316-318) and it was decided to test it in the estimation of geoidal undulations at the grid points. Sjöberg shows that the optimum value for ν is about 3.5 (Ibid.), and tests were performed with the Alaska Data Set to see what effect the use of this simple model would have on the resultant map. Two values of ν were tested ($\nu = 1$ and $\nu = 3.5$) for both a 5 data points and a 10 data points prediction. It was found that, in this case, the value of ν had little influence on the resulting prediction. The use of 5 data points in the prediction was about 20% less expensive than 10 data points (whose cost was comparable to that of the least squares prediction). However, there appeared to be little advantage in using 10 points in the prediction as the resulting values were significantly unchanged.

An example of the maps produced by the simple weighted mean method is given in Figure 3.

Errors in the Predicted Quantities

The error in the predicted value (σ_r) will come from two sources, (i) the error in the data (σ_d) and (ii) the error of representation of the weighted mean (σ_p). These two errors are uncorrelated for all practical purposes, and the total prediction error is expressed as:

$$\sigma_r^2 = \sigma_p^2 + \sigma_d^2 \quad (3.1)$$

σ_d can be gauged from an analysis of the differences of each predicted value from the mean value. Thus:

$$\sigma_d^2 = \frac{\sum_i p v v}{\sum_i p\,(n-1)} \quad (3.2)$$

where

$$\begin{aligned} i &= 1 \text{ to no. of points used in prediction} \\ \text{and} \quad p_i &= 1/r_i^{\nu} \\ r_i &= \text{separation of point } i \text{ from the prediction point.} \end{aligned}$$

σ_p is related to either the size of the area for which the predicted value represents a mean value, or the 'distances' over which the prediction is made. In both cases, a function of distance (d') is involved, and thus we can say:

$$\sigma_p^2 = c\, d'$$

For convenience in this case (since this quantity was already computed)

$$d' = \sum_i r_i^{-1} \tag{3.3}$$

and by experiment c was found to be about 30 m^3.

The final result

$$\sigma_r^2 = \frac{\sum_i p v v}{\sum p(n-1)} + 30 \sum_i p_i$$

was used to estimate the error of prediction at each grid point and the resultant map of the errors showed the same trends as for the least squares error analyses (compare Tables 3 and 5, and Figures 2 and 4). Table 5 and Figure 4 are derived from 10 data points in the prediction of each grid value. The errors estimated using 5 data points are considerably higher, as might be expected, although the actual estimates of N are significantly the same.

The differences between the least squares prediction and the weighted mean (with 10 points) gives an RMS of about 1.5 m. In areas where the data is comparatively dense (see Figure 1) the differences are small (compare, for example, rows 7 and 8 in Table 4 and Table 2), but in some instances they are unacceptably large. For example, point (16, 8) is 0.0 in Table 2 and -13.8 in Table 4. This occurs in an area of no data and reflects the weakness of the methods when applied

Figure 1

Prediction by Least Squares of Geoid Undulations
Alaska Test Area

Contour Interval: 5 m
Projection: Cassini-Soldner
Grid: 21 x 11

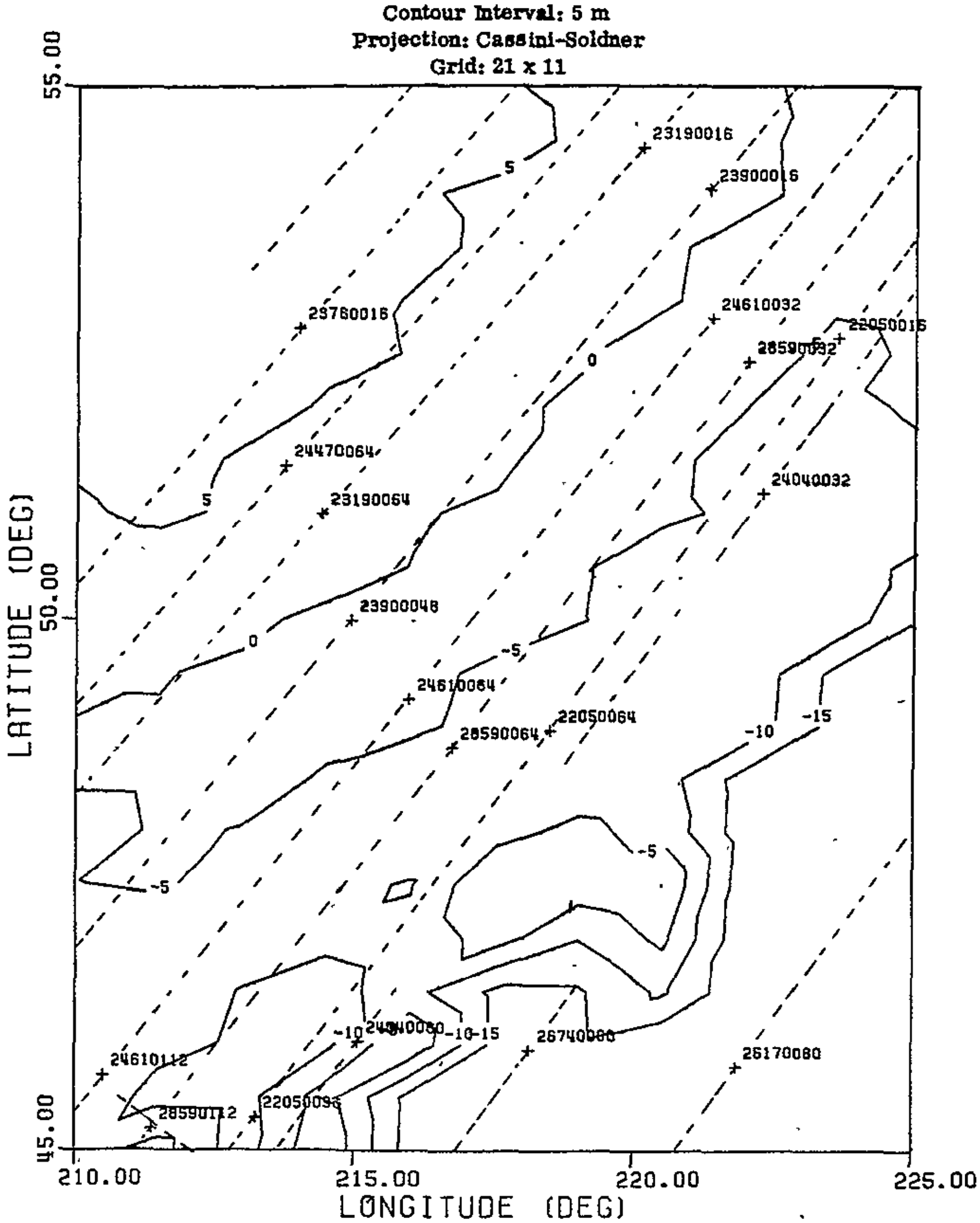

Figure 2

Precision of Least Squares Prediction
Alaska Test Area

Contour Interval: 1 m

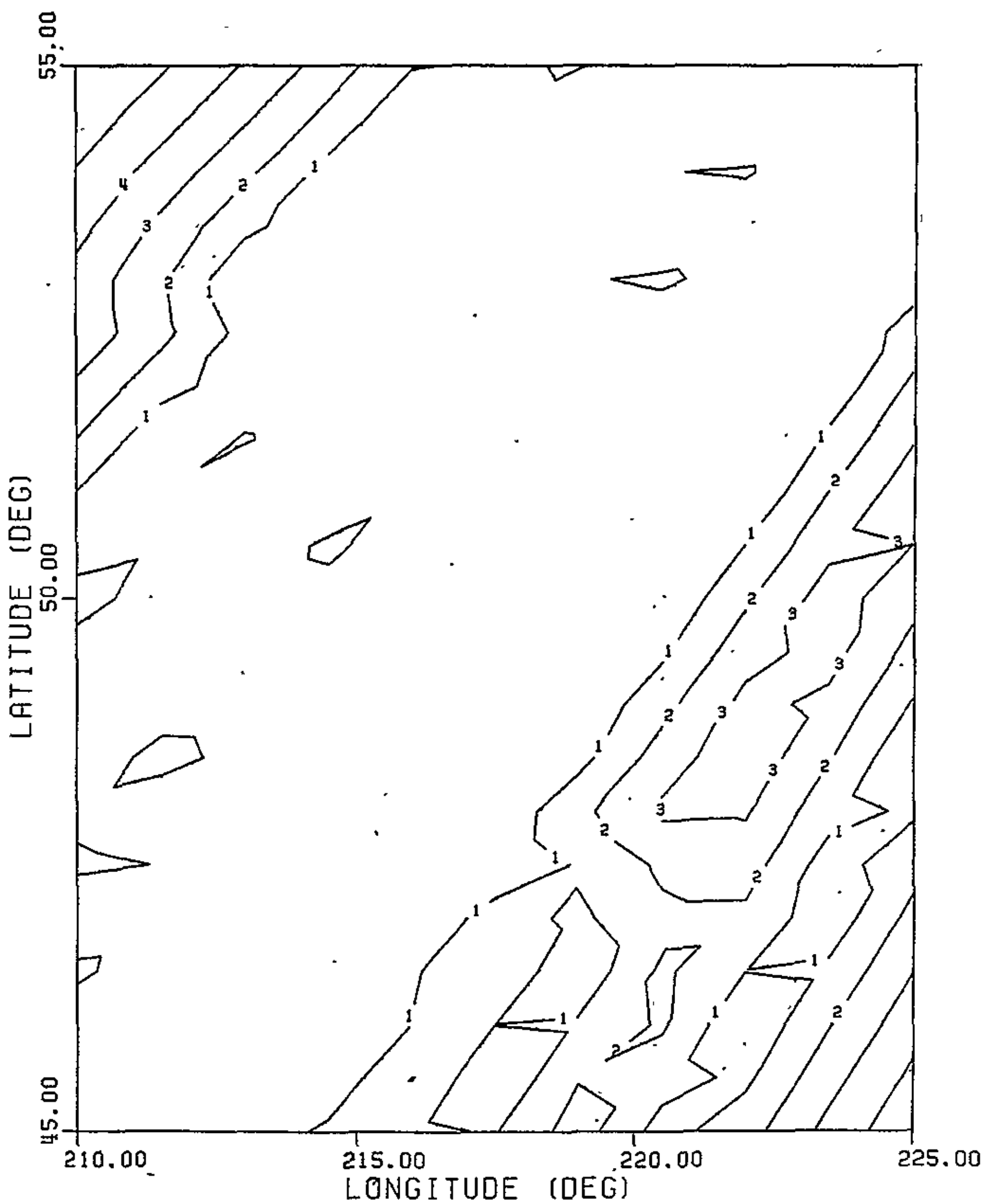

Figure 3

Geoidal Undulations For Alaska Test Area Using Weighted Means

Contour Interval: 5 m
Projection: Cassini-Soldner
Grid: 21 x 11

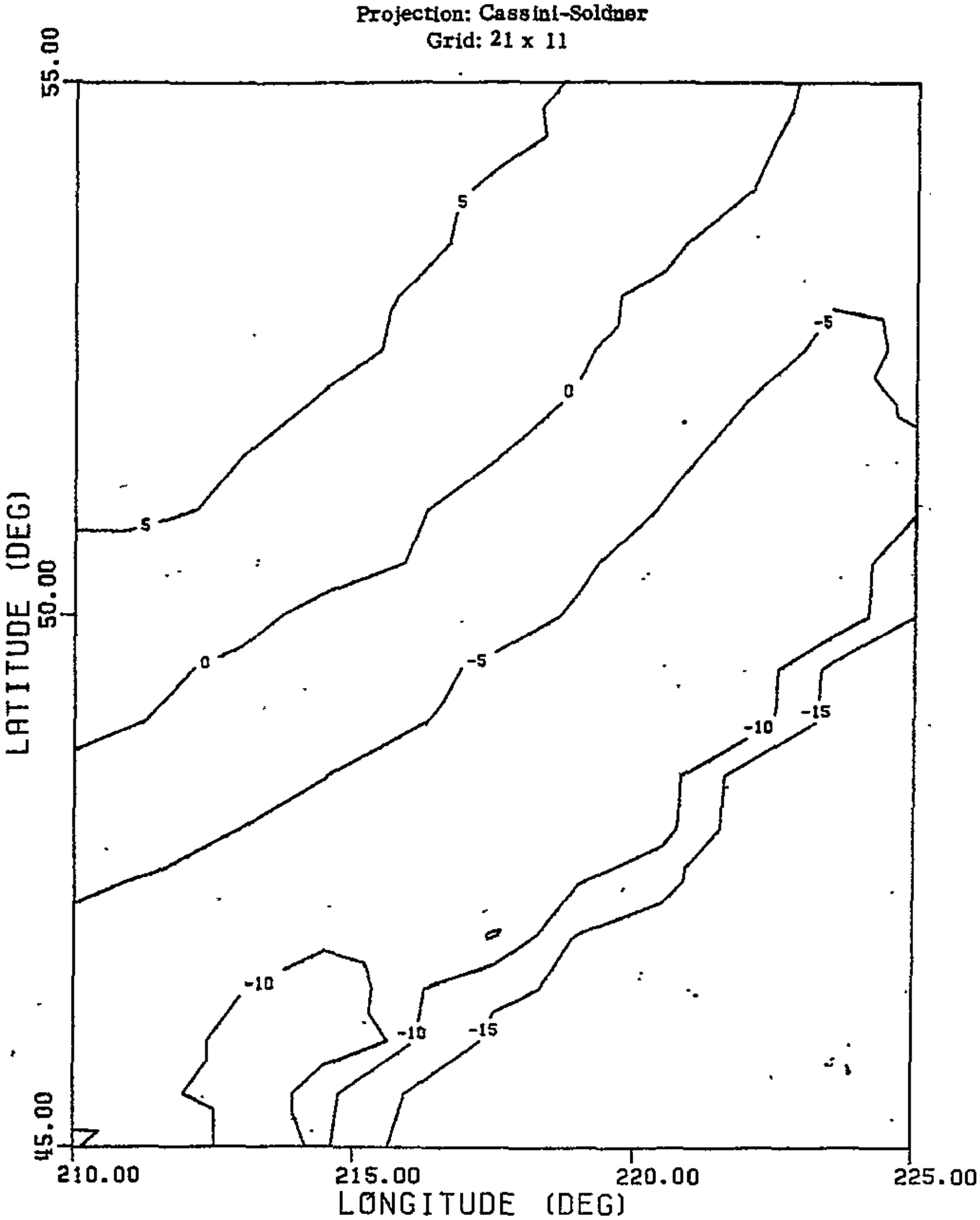

Figure 4

Precision of Prediction by Weighted Means
Alaska Test Area

Contour Interval: 1 m

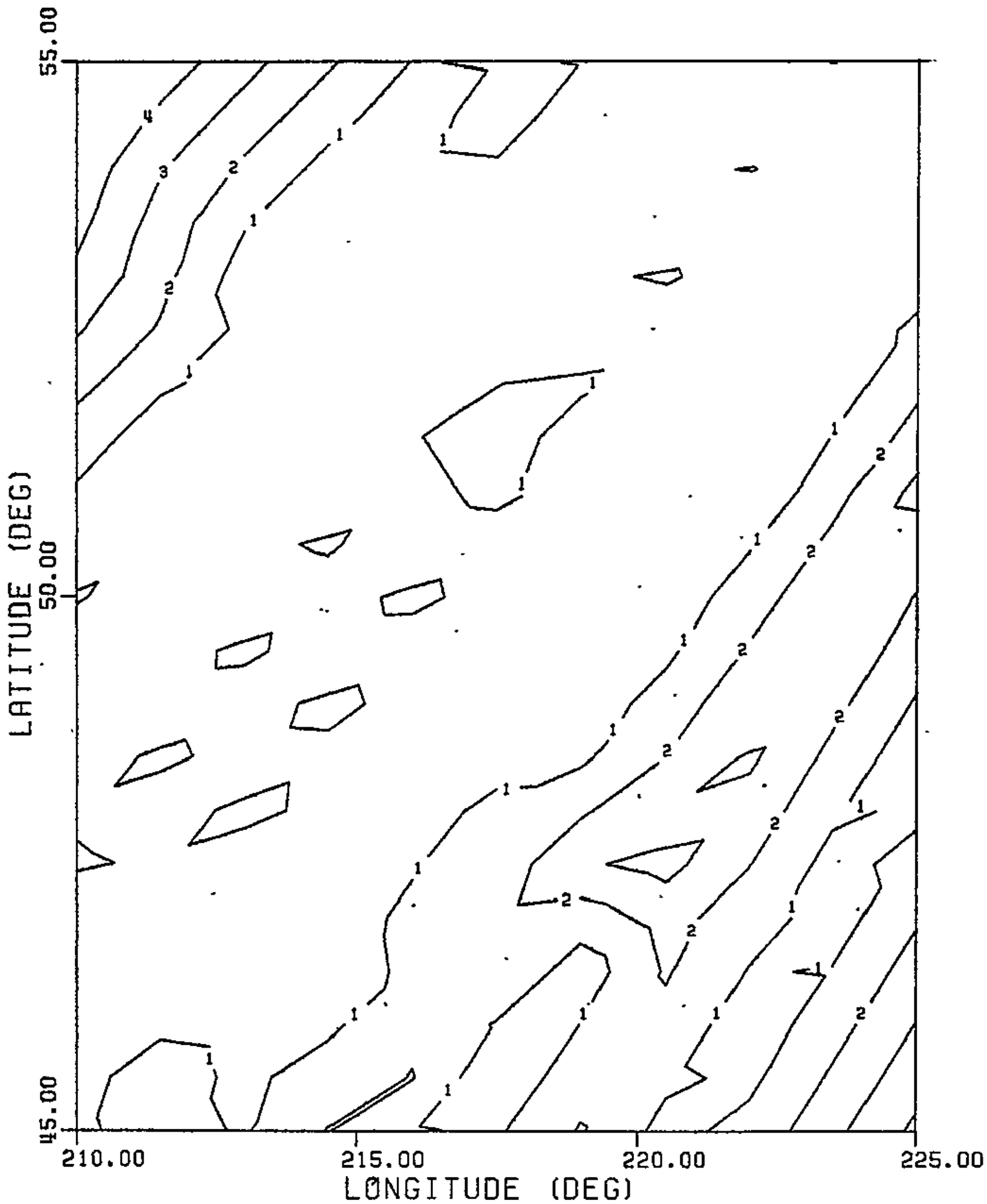

Table 2

Table of Predicted Geoid Heights by Least Squares Prediction

Alaska Test Area

	1	2	3	4	5	6	7	8	9	10	11
1	8.9	8.9	8.8	8.8	9.2	5.4	3.9	3.2	0.8	-1.3	-2.7
2	7.5	9.0	9.0	8.8	8.9	6.7	4.1	3.0	1.2	-2.2	-3.7
3	7.0	8.0	9.1	9.0	5.4	4.2	2.9	1.1	1.2	-2.0	-4.0
4	6.4	7.4	9.2	8.1	6.0	4.2	2.7	0.8	-2.3	-2.7	-4.6
5	7.3	6.6	8.2	6.5	4.7	2.7	0.3	0.5	-2.6	-4.7	-4.3
6	6.1	6.2	6.5	5.8	4.9	2.9	0.5	-2.7	-3.8	-5.7	-4.6
7	5.8	6.2	6.3	4.6	3.3	1.0	-0.9	-2.7	-5.1	-5.2	-4.9
8	5.4	6.2	4.6	3.8	3.1	1.0	-2.7	-4.2	-6.5	-5.4	-5.1
9	4.6	5.7	4.4	2.4	0.4	-0.8	-2.7	-4.4	-5.8	-5.6	-5.4
10	3.3	3.5	2.4	2.1	-0.1	-2.8	-4.6	-7.0	-6.0	-5.8	-11.9
11	2.5	3.0	0.9	-1.0	-2.1	-3.2	-4.8	-6.6	-6.2	-5.9	-14.9
12	1.4	0.2	-0.6	-1.4	-4.0	-5.8	-7.8	-6.8	-6.4	-16.0	-15.5
13	-0.3	-0.2	-2.3	-3.5	-4.3	-6.2	-8.0	-7.3	-6.8	-16.6	-16.1
14	-3.8	-3.4	-2.7	-5.5	-7.1	-9.2	-7.2	-7.8	-17.5	-17.2	-16.7
15	-9.0	-4.0	-5.2	-5.9	-7.6	-6.2	-4.0	-6.5	-18.0	-17.6	-17.2
16	-5.1	-4.6	-6.2	-8.8	-10.3	-0.1	-2.4	0.0	-18.5	-18.0	-17.7
17	-7.0	-7.7	-7.1	-9.3	-8.4	-3.0	-9.9	-4.0	-18.9	-18.5	-18.1
18	-8.6	-8.1	-10.1	-11.3	-8.3	-15.9	-15.7	-9.2	-19.3	-18.9	-18.5
19	-8.8	-8.4	-10.6	-11.5	-0.2	-16.1	-15.9	-19.6	-19.5	-19.2	-18.9
20	-5.8	-11.6	-12.2	-2.9	-16.6	-16.3	-16.1	-19.7	-19.6	-19.4	-19.1
21	-8.1	-3.0	-12.6	-0.9	-16.9	-16.6	-16.4	-19.8	-19.7	-19.5	-19.3

Table 3

Table of Predicted Standard Errors

Alaska Test Area

	1	2	3	4	5	6	7	8	9	10	11
1	6.3	5.2	3.9	2.6	1.0	0.9	1.1	0.3	1.0	0.5	0.8
2	5.6	4.4	3.1	1.7	0.2	0.8	0.0	0.5	0.1	0.3	0.2
3	4.9	3.6	2.2	0.6	0.2	0.8	0.5	1.0	1.1	0.3	0.3
4	4.3	2.8	1.3	0.3	0.9	0.3	0.6	0.1	0.4	0.1	0.2
5	3.7	2.1	0.2	0.1	0.6	0.4	0.9	1.1	0.7	0.3	0.5
6	3.7	2.3	0.7	0.5	0.6	0.8	0.3	0.5	0.1	0.1	1.4
7	2.9	1.4	0.5	0.3	0.1	0.8	0.6	0.6	0.4	0.3	2.2
8	2.0	0.3	1.1	0.4	1.0	0.5	0.5	0.2	0.1	1.2	2.9
9	1.0	0.9	0.0	0.1	0.8	0.6	0.6	0.9	0.0	2.0	3.6
10	0.3	0.8	0.4	1.2	0.4	0.5	0.3	0.2	1.0	2.7	3.0
11	1.5	0.4	0.4	0.6	0.6	0.6	0.7	0.1	1.8	3.4	2.4
12	0.5	0.5	0.6	0.6	0.5	0.4	0.4	0.8	2.6	3.4	1.7
13	0.6	0.6	0.5	0.6	0.6	0.7	0.2	1.7	3.3	2.8	0.9
14	0.3	1.3	0.7	0.5	0.5	0.5	0.7	2.5	3.7	2.1	0.1
15	0.7	0.3	0.9	0.6	0.6	0.3	1.7	3.2	3.1	1.4	0.8
16	1.2	1.0	0.2	0.5	0.6	0.4	1.1	2.2	2.5	0.6	1.6
17	0.2	0.4	0.7	0.6	0.2	1.4	0.8	1.8	1.8	0.4	2.3
18	1.3	0.2	0.5	0.7	0.9	1.8	0.2	2.2	1.0	1.2	3.0
19	0.2	0.7	0.6	0.4	1.0	1.0	1.1	2.1	0.2	1.9	3.6
20	0.3	0.5	0.8	0.3	2.0	0.1	1.9	1.4	0.8	2.6	4.2
21	0.7	0.0	0.3	1.2	1.2	0.9	2.5	0.6	1.6	3.3	4.8

Table 4

Table of Predicted Geoid Heights by Weighted Means:

$\nu = 1$

(10 Closest Points)

	1	2	3	4	5	6	7	8	9	10	11
1	9.2	9.1	8.9	8.9	9.2	9.1	3.9	3.2	1.5	-1.1	-3.0
2	9.2	9.2	9.0	8.9	8.9	6.2	4.1	3.0	1.1	-2.3	-3.6
3	9.2	9.2	9.1	9.0	6.8	4.2	3.2	1.7	0.1	-2.0	-4.6
4	8.4	9.0	9.2	8.2	5.8	3.9	2.7	0.8	-2.2	-2.7	-4.6
5	7.2	8.0	9.0	6.5	4.7	2.9	0.6	-0.7	-2.9	-4.8	-4.5
6	6.1	6.6	6.9	5.9	4.5	2.8	0.5	-2.7	-3.7	-5.7	-4.6
7	6.2	6.2	6.3	4.7	3.3	1.6	-0.5	-3.0	-5.1	-5.3	-4.9
8	5.9	6.1	5.0	3.8	2.8	0.1	-2.7	-4.1	-6.3	-5.4	-5.2
9	5.5	5.5	4.4	2.4	0.3	-1.3	-3.0	-5.2	-5.8	-5.6	-9.6
10	4.3	3.4	2.3	1.4	-0.1	-2.9	-4.5	-6.8	-6.1	-5.7	-14.4
11	3.3	2.8	1.0	-1.0	-2.1	-3.5	-5.5	-6.7	-6.2	-6.0	-15.0
12	2.1	0.5	-0.6	-1.4	-4.0	-5.7	-7.7	-6.9	-6.4	-16.1	-15.5
13	1.1	-0.2	-2.3	-3.5	-4.6	-6.6	-8.0	-7.3	-6.8	-16.7	-16.1
14	-0.9	-2.6	-2.5	-4.9	-7.0	-8.8	-8.4	-7.8	-17.6	-17.1	-16.7
15	-1.5	-4.0	-5.0	-6.3	-7.9	-7.7	-7.4	-8.2	-18.1	-17.6	-17.3
16	-4.6	-5.2	-6.8	-8.5	-9.7	-5.5	-9.8	-13.8	-18.4	-18.1	-17.6
17	-5.5	-7.8	-7.6	-9.5	-8.7	-4.6	-15.1	-16.8	-18.9	-18.5	-18.1
18	-6.6	-8.1	-9.9	-11.1	-9.1	-14.1	-15.7	-17.0	-19.3	-18.9	-18.6
19	-7.7	-9.0	-10.7	-11.0	-9.6	-16.1	-15.9	-19.6	-19.5	-19.3	-18.9
20	-9.1	-9.0	-12.1	-8.8	-15.4	-16.3	-16.1	-19.7	-19.6	-19.5	-19.3
21	-10.4	-5.3	-12.1	-9.4	-16.9	-16.6	-18.4	-19.8	-19.7	-19.6	-19.5

Table 5

Table of Predicted Standard Errors, by Weighted Means

$\nu = 1$

(Using 10 Closest Points)

	1	2	3	4	5	6	7	8	9	10	11
1	5.9	4.6	3.3	2.1	1.0	1.1	1.0	0.6	0.9	1.0	0.7
2	5.2	3.8	2.6	1.4	0.4	1.6	0.3	0.6	0.3	0.5	0.5
3	4.6	3.1	1.8	0.7	0.7	0.8	0.6	0.9	1.0	0.7	0.7
4	4.3	2.6	1.1	0.8	0.8	0.5	0.7	0.3	0.6	0.3	0.4
5	3.8	2.3	0.5	0.4	0.7	0.5	0.9	1.1	0.7	0.8	0.6
6	3.1	1.9	0.8	1.0	0.7	0.8	0.4	0.6	0.4	0.4	1.2
7	2.3	1.2	0.6	0.5	0.4	1.0	1.1	0.7	0.8	0.5	1.8
8	1.5	0.5	1.0	0.8	0.9	1.4	0.6	0.5	0.4	1.1	2.4
9	0.9	0.9	0.3	0.4	0.8	1.2	0.7	0.8	0.2	1.6	3.3
10	0.4	0.8	0.8	1.1	0.6	0.6	0.5	0.4	0.9	2.3	2.5
11	1.1	0.6	0.5	0.7	1.2	0.7	0.8	0.4	1.5	2.9	1.9
12	0.6	0.7	1.2	0.6	0.6	0.6	0.5	0.8	2.1	2.8	1.4
13	0.8	0.7	0.6	1.2	0.7	0.8	0.5	1.4	2.8	2.3	0.9
14	0.5	1.2	0.7	0.8	0.6	0.8	0.8	2.0	3.2	1.7	0.4
15	0.9	0.5	1.3	0.8	0.7	1.2	1.9	2.9	2.6	1.2	0.8
16	1.1	0.9	0.5	0.7	0.9	1.4	2.9	3.3	2.0	0.7	1.3
17	0.4	0.5	0.8	0.7	1.1	1.7	1.5	2.4	1.5	0.5	1.9
18	0.9	0.5	0.7	0.7	1.1	2.0	0.4	2.1	0.9	1.1	2.5
19	1.0	0.8	0.7	0.8	1.8	0.9	1.0	1.7	0.4	1.6	3.0
20	0.7	1.4	0.8	1.5	2.0	0.2	1.6	1.2	0.8	2.2	3.6
21	0.9	1.3	0.9	2.0	1.1	0.9	2.1	0.7	1.3	2.7	4.2

to a situation requiring extrapolation. It appears that, providing the area is densely covered by data, a simple weighted mean approach produces quite adequate results. However, the total cost of the prediction are similar, and the advantage of using the least squares method is that it provides a super-structure of theory which is lacking in the more intuitive weighted means approach and also, that it simplifies the computation of the expected error of the prediction.

4. Choosing the Grid Interval for Contouring

The usual specifications for a medium to large contour map is that contour interval (I) be between $3.33\,\sigma_H$ and $5\,\sigma_H$, where σ_H is the standard deviation of the individual heights in the mapping area (Richardus, 1973, p. 83). While the maps involved here can hardly be considered medium or large scale, it is considered reasonable to adopt as the standard $I = 2\sigma_H$, as the comparative smoothness of the geoid over large areas makes it unfeasible to apply small scale standards to this problem. The internal consistency of the altimetry data gauged from the discrepancies in the crossover points after adjustment (see Rapp, 1977) suggests a σ_H of about 0.5 m, but it appears that a contour interval of less than 2 m would be unrealistic. In fact, in earlier tests a contour interval of 5 m was used, but with the refinement of the technique, 2 m was finally adopted.

In normal topographic mapping the contours are either interpolated linearly between points defined by field survey at changes of grade, or are plotted directly from a three dimensional photographic model. The criteria applied in these two cases are not helpful in this present instance, where the contouring will be done from height values predicted on a pre-determined grid pattern. The problem is to find the optimum grid pattern which will:

(i) faithfully represent the mapping area in a discrete form
(ii) produce realistic contour lines
(iii) not be too costly.

The first point is probably the most important. Too large a grid interval will leave large areas of the map unrepresented. The subsequent contour lines, being a simple linear interpolation between grid points will therefore miss the features present in the ungridded data, since the grid points lack the important property of being located at salient points which adequately describe the features of the geoid. The extreme is to make the grid spacing equal to the separation of the altimeter data along any one track ($\simeq 0.3$ degrees) but such an intensive grid would be very costly to predict and map and is unnecessarily dense.

The normal criterion for contour line accuracy is that it be accurate to within $\pm 1/3$ I, I being the contour interval. An accuracy of 0.7 m is bordering on the noise level of the altimeter data, and it seems more realistic to prescribe an accuracy of 1 m for the contour line. This means that a grid interval should be chosen so that it is less than half the wavelength of geoidal undulations having amplitudes of at least 1 m (Nettleton, 1976, p. 159).

This wavelength will obviously vary from area to area, and it is difficult to determine its magnitude without some a priori knowledge of the areas. One could use existing geoid maps for ocean regions such as the U. S. Calibration Area, but these maps themselves will be limited in accuracy by the grid interval chosen as the basis for the map. A study of the adjusted altimetry may reveal some of the wavelength characteristics of the geoid in the mapping area. Failing all else, the grid interval can be determined by trial and error.

Tests with various grid intervals showed a value of 2° failed to sense high frequency features related to the ridge and trench systems on the ocean floor. A 1° grid appeared to be adequate to represent these features and did not increase the cost of the maps beyond reasonable limits. In any case, a 1° spacing seems to be the smallest that could reasonably be used, as spectral analysis of altimeter data suggests that below a 100 km half wavelength, the sea surface topography seems certain to be dominated by sea state departures (Wagner, 1977, p. 35). With all cost reducing options operating, the cost of producing a $30^\circ \times 30^\circ$ geoid map and its associated error map from about 3500 altimeter data was $\simeq$ \$15.

Some comments concerning the maps of precision are warranted here. It must be recognized that these are derived from the expected error of prediction (Moritz, 1972, Eq. 4-28a) at the grid points. They are thus maps of the precision of prediction at the grid points and <u>may</u> not reflect the actual precision of values interpolated between grid points (particularly if the grid interval is too large to sense the high frequency features). Also, they do not reflect the accuracy of the contours of the geoid map. This, if the grid interval has been properly chosen and the data coverage is adequate, should be of the order of ± 1m, as explained above.

The accuracy of the contours will, in the final analysis, be dependent upon the algorithms used in the computer program to interpolate the contour lines between the grid points. The routine used in this case (Subroutine CGTOUR, Snowden, 1969) joins interpolated points by a series of short straight lines. This gave rise to a peculiar 'stepping' or 'staircasing' effect in areas where the grid points lay between two widely (i.e. 2°) separated arcs. This was because grid points close to one arc used only points from that arc to determine its value, while those closer to the second used only data from that arc. In an attempt to overcome this problem, a condition was imposed whereby of the five close points chosen to provide data for prediction, only the first three could come from the closest arc and the remainder had to be chosen from other arcs.

5. The Predicted Geoid - Results and Accuracies

The errors computed in Sections 3.1 and 3.2 estimate the precision or the internal accuracy of the prediction. To obtain some estimate of the absolute accuracies of prediction, a comparison of the predicted geoid undulations at 1° intervals was made with existing geoid values in (i) the U. S. Calibration Area, and (ii) the Philippines region of the Pacific Ocean. The results of the comparison are summarized below.

5.1 Accuracy of the Geoid from Altimetry

(i) U. S. Calibration Area

The altimeter geoid has been compared with two different geoids in the area bounded by $40° \geq \varphi \geq 20°$ and $297° \geq \lambda \geq 277°$. The geoids used for comparison were (i) that described by Rapp and Rummel (1975), where the GEM 6 coefficients were combined with the 1° x 1° anomaly data and (ii) the geoid computed by Marsh and Chang (1976) who combined the potential coefficients of GEM 8 with 1° x 1°, 15' x 15' and 5' x 5' mean anomalies.

Table 6

Undulation Comparisons in GEOS-3 Calibration Area

	$N_{ALT} - N_{R,R}$	$N_{ALT} - N_{M,C}$
Mean Difference	-0.3 m	-1.0 m
RMS Difference	±1.2 m	±1.5 m
$[\text{Variance}]^{\frac{1}{2}}$	±1.2 m	±1.1 m
Number	337	335
Maximum Difference	5.0 m	9.2 m
Minimum Difference	-3.5 m	-4.6 m

The values in Table 6 should be viewed in the light of the expected accuracies of the $N_{R,R}$ and $N_{M,C}$ values. The standard deviations of $N_{R,R}$ range from 1.1 m to 2.1 m, with a mean of about 1.6 m, so much of the contribution in the differences will come from the $N_{R,R}$ value. A similar comment can be made concerning the $N_{M,C}$ values.

A plot of the differences shows a systematic trend or slope exists between the altimetry geoid and the Rapp, Rummel and Marsh, Chang geoids. This could indicate small errors in the potential coefficient sets used in the analysis (Rapp, 1977, p. 13). However, the comparisons seem remarkable considering the fact that the N_{ALT} contains instrumental noise, and is in reality a map of sea surface topography rather than the geoid. The comparison indicates that the original estimates of accuracy and the plotting parameters based thereon (Sections 1.1 and 4) are acceptable for continued mapping.

(ii) Philippines Area (see Figure 6)

Differences were taken between the altimetry undulation values and those supplied by Marsh (1977, private communication) at $1^\circ \times 1^\circ$ intersections in the Philippines area. Analysis of 625 differences showed that the average value was -1.33 m (N_{ALT} - N_{MARSH}), with an RMS value of ±4.0 m. Upon removing the mean difference from these differences, a standard deviation of ±3.75 m was obtained. Maximum positive difference was 7.4 m while maximum negative difference was -13.3 m.

The area has a number of high-amplitude features of relatively short wavelength ($\simeq 3^\circ$) and it is unlikely that these features would be reflected in the gravimetrically derived geoid of Marsh. This helps to explain why the comparison in this region is not as favorable as that in the U. S. Calibration Area.

5.2 Results of Computations

The techniques developed above were now applied to adjusted altimetry data in the Pacific, Indian and Atlantic Oceans. A basic area of $30^\circ \times 30^\circ$ was chosen for mapping (see Figure 5 and Table 7) and the geoid maps themselves, with their associated precision maps, are presented in Figures 6 to 45. It is felt that for most purposes these maps should provide good service for years to come. Areas of the oceans not portrayed in these individual maps did not have sufficient altimetry data available at the time of the report preparation to warrant the production of the contour maps.

Figure 5

Index of Geoid Maps from Geos-3 Altimetry

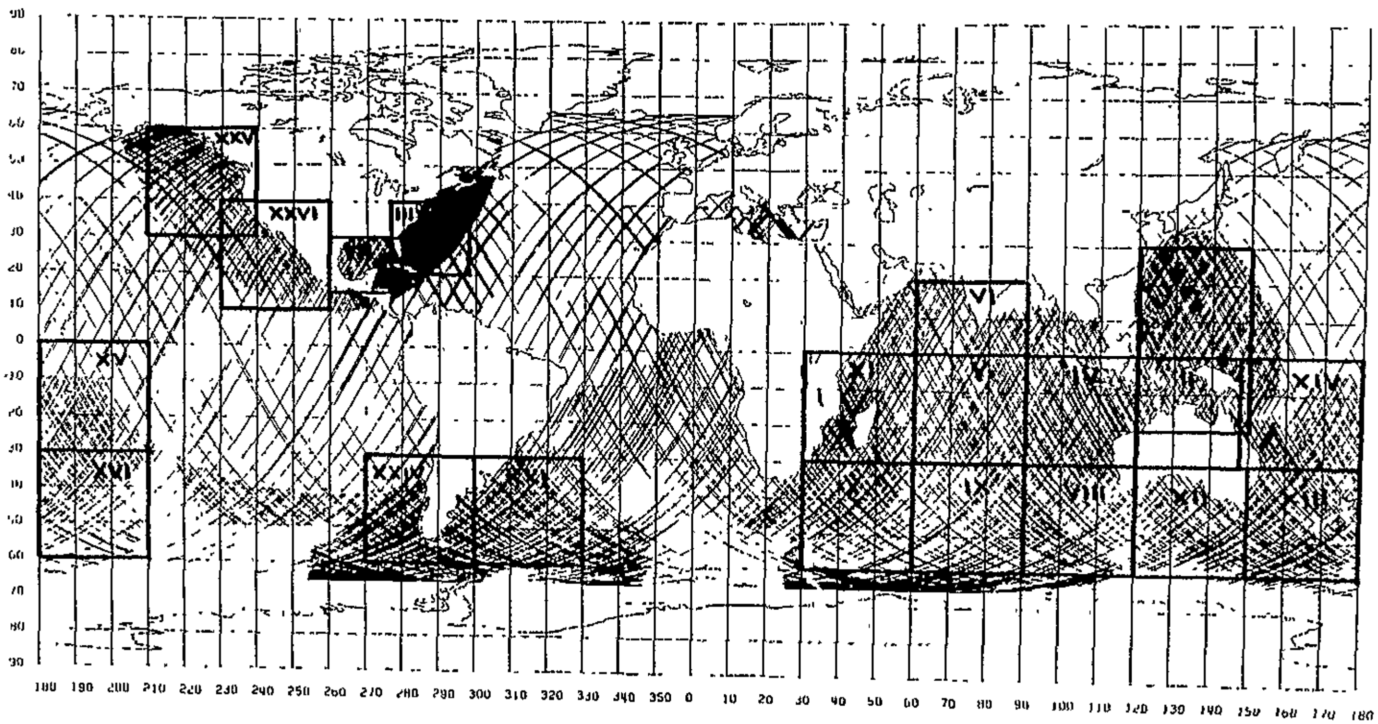

Table 7

Index - Geoid Maps from Altimetry

Map No.	Fig. No.	Geog. Limits		Description
		Lat. (degrees)	Long. (degrees)	
I	6	30 → 0	150-120	Philippines - W. Pacific
II	8	0 → -20,	150-120	New Guinea - N. Australia
III	10	40 → 20,	297-277	U. S. Calibration Area
IV	12	0 → -30,	120- 90	Indonesia-East Indian Ocean
V	14	0 → -30,	90- 60	Central Indian Ocean
VI	16	20 → 0,	90- 60	India - N. Central Indian Ocean
VII	18	30 → 15,	280-260	S. W. U. S. Calibration Area
VIII	20	-30 → -60,	120- 90	S. E. Indian Ocean - S. W. Australia
IX	22	-30 → -60,	90- 60	S. Central Indian Ocean
X	24	-30 → -60,	60- 30	S. W. Indian Ocean
XI	26	0 → -30,	60- 30	East Africa - W. Indian Ocean
XII	28	-30 → -60,	150-120	South Australia Basin
XIII	30	-30 → -60,	180-150	New Zealand - Tasman Sea
XIV	32	0 → -30,	180-148	N. E. Australia - Coral Sea
XV	34	0 → -30,	210-180	Mid Central Pacific Ocean
XVI	36	-30 → -60,	210-180	S. Central Pacific Ocean
XXI	38	-30 → -60,	330-300	S. West Atlantic
XXIV	40	-30 → -60,	300-270	South America
XXV	42	60 → 30,	240-210	N. E. Pacific
XXVI	44	40 → 10,	260-230	N. E. Pacific

Figure 6

Geoid Undulations in the Philippines
From Adjusted Altimeter Data
Contour Interval: 2 meters
Grid Interval 1°
Scale 1: 500,000

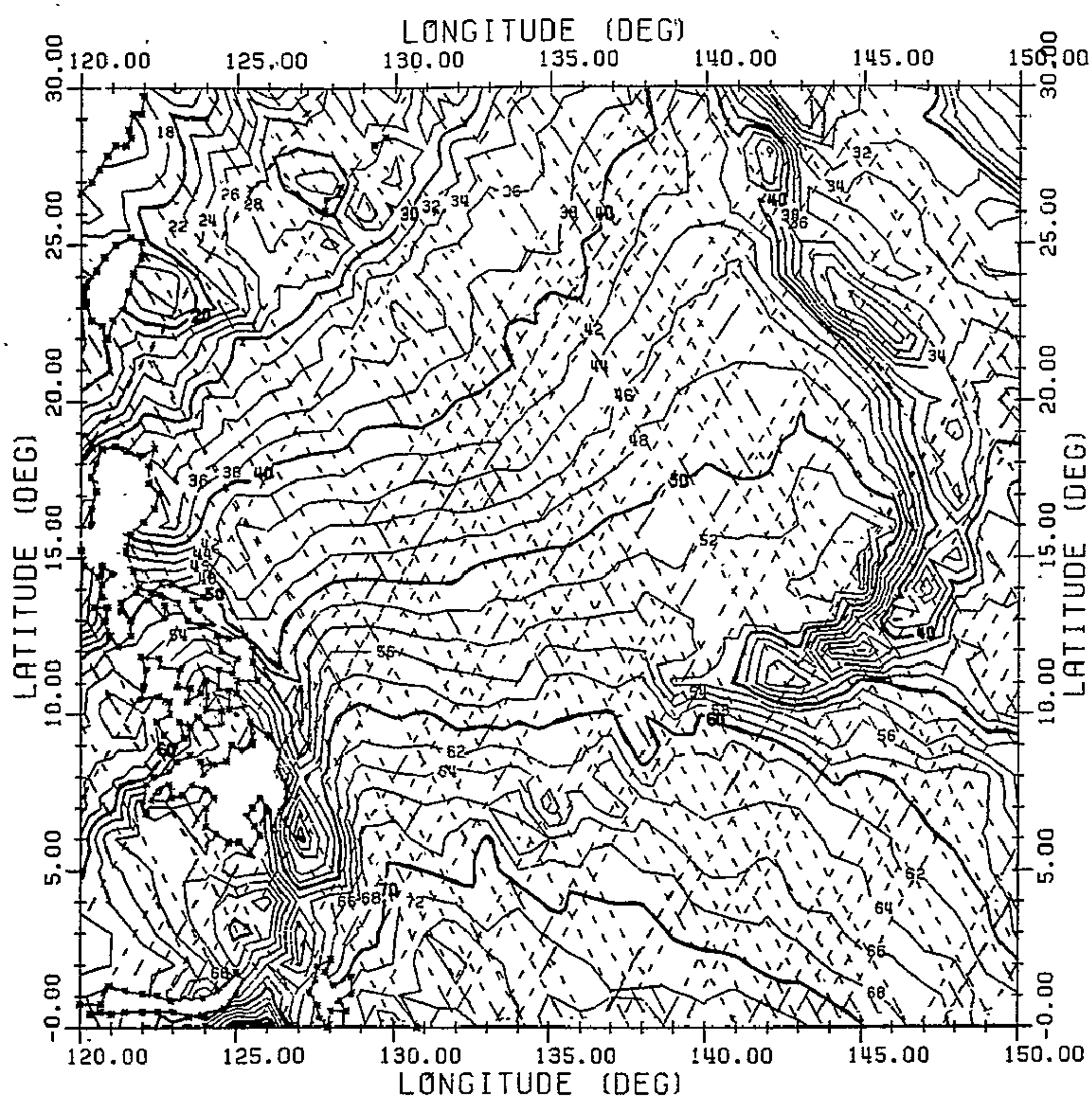

ORIGINAL PAGE IS
OF POOR QUALITY

Figure 7

Geoid Undulation Accuracy in the Philippines
From Adjusted Altimeter Data.
Contour Interval: .5 meters
Grid Interval 1°
Scale 1: 500,000

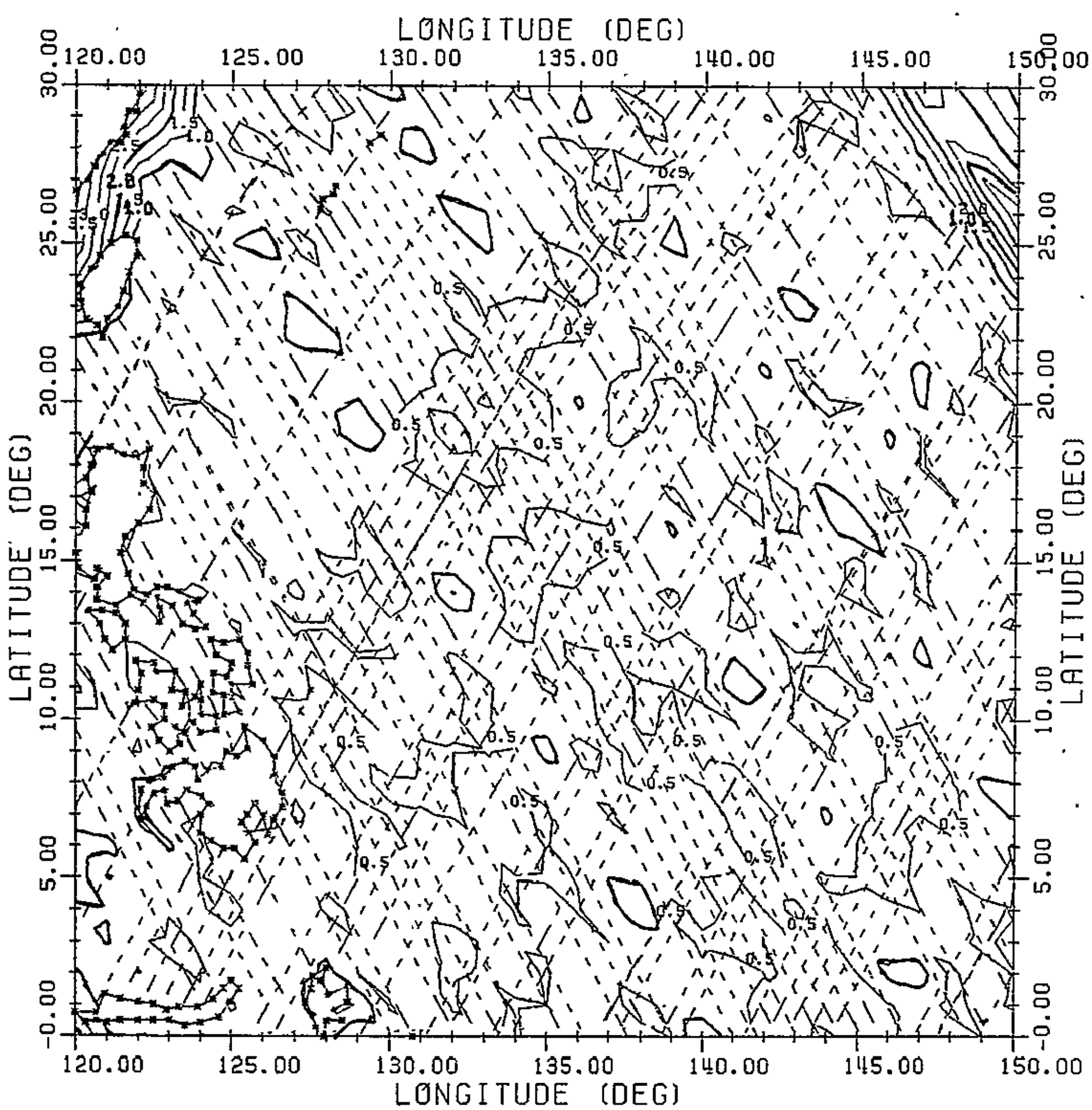

Figure 8

Geoid Undulations - New Guinea

Grid Interval 1°
Contour Interval 2 m
Scale 1: 500,000

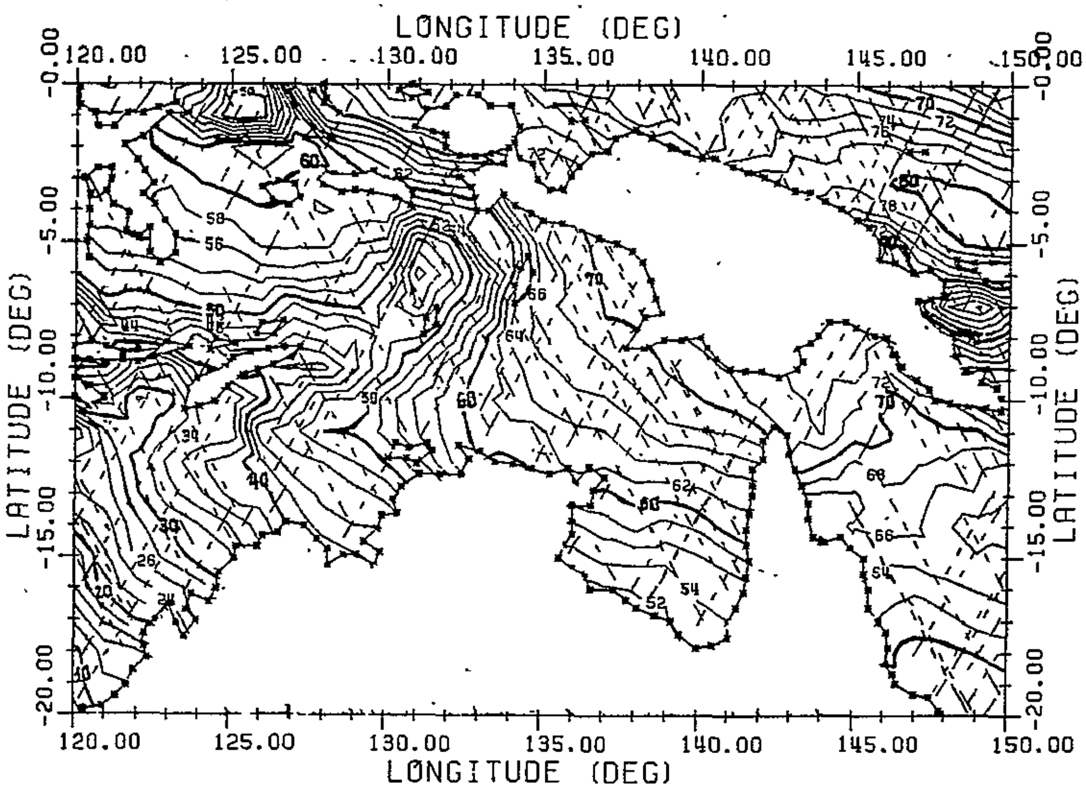

Figure 9

Precision of Prediction - New Guinea

Grid Interval 1°
Contour Interval 0.5 m
Scale 1: 5,000

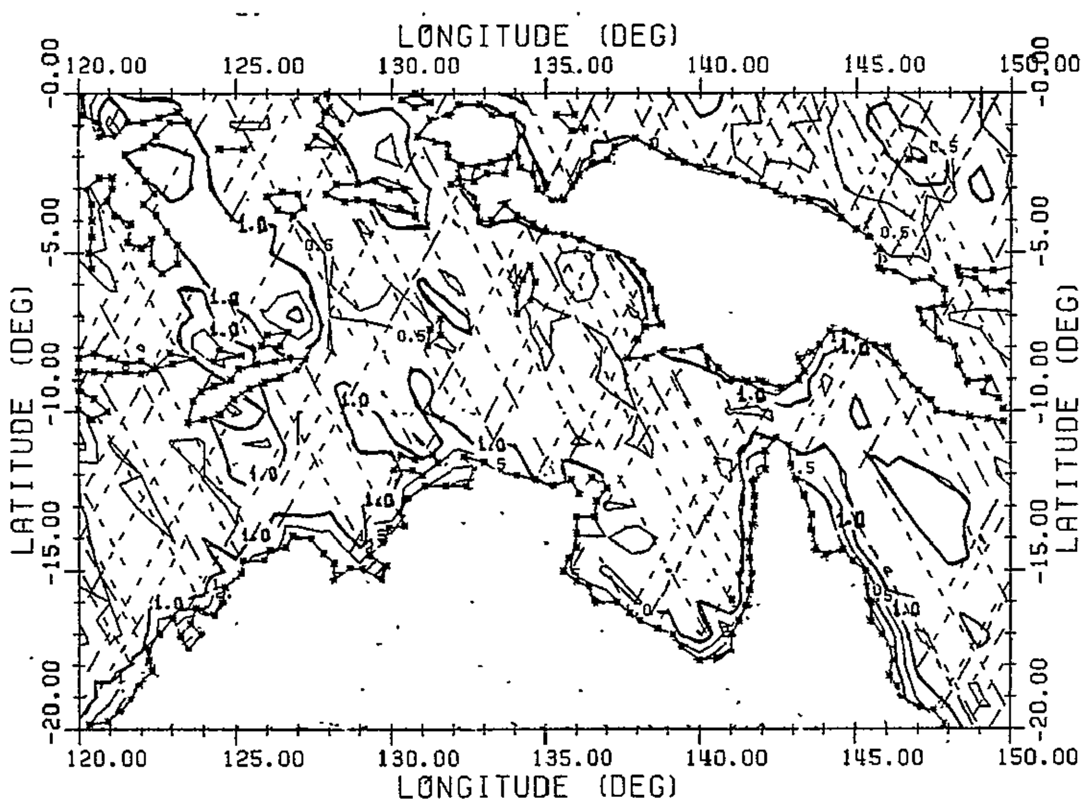

Figure 10. Geoid Undulations in Geos-3 Calibration Area
From Adjusted Altimeter Data.
(Contour Interval: 2 meters)
Grid Interval 1°
Scale 1: 333,333

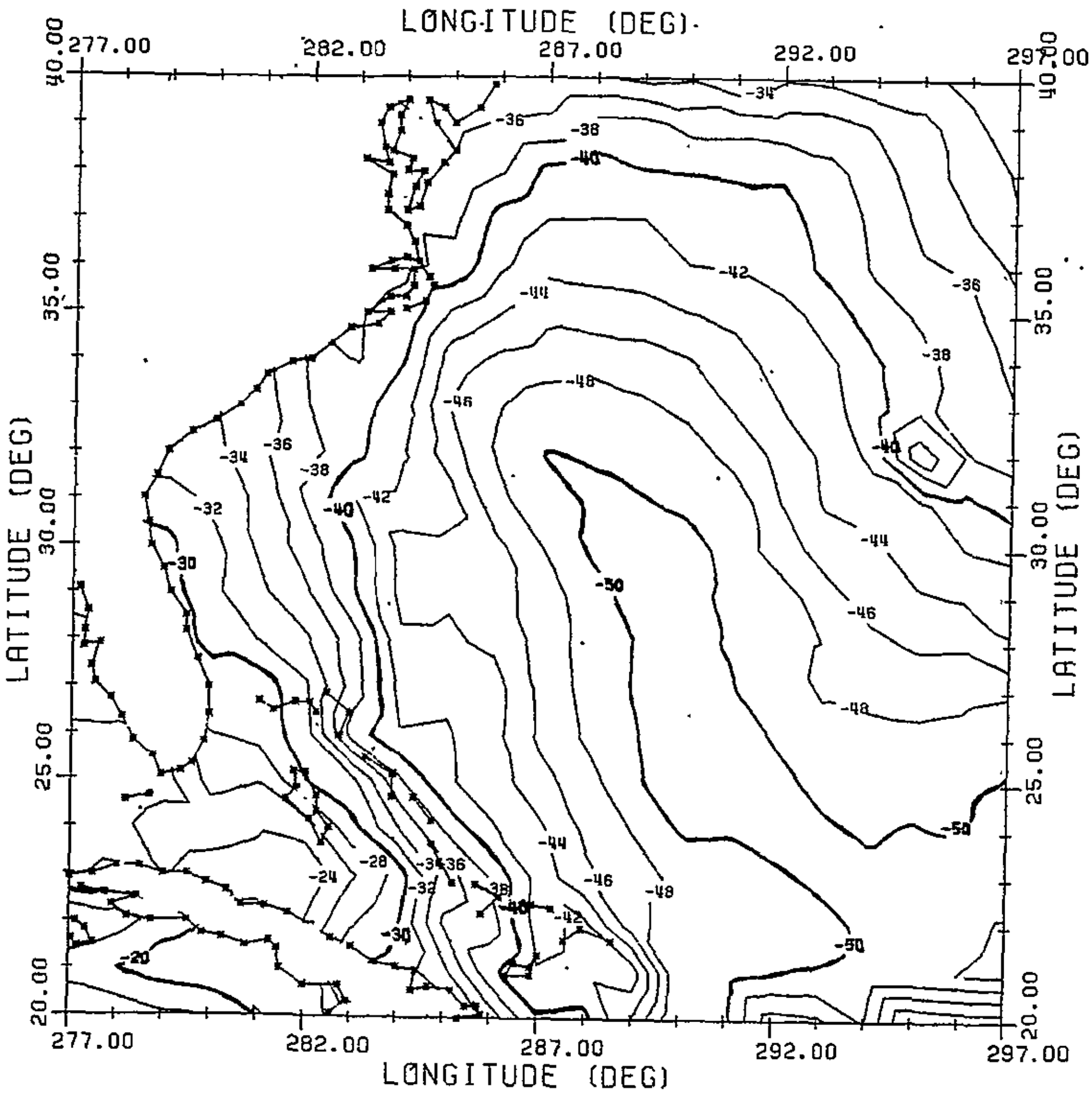

Figure 11. Geoid Undulation Accuracy in Geos-3 Calibration Area
From Adjusted Altimeter Data.
(Contour Interval: 0.5 meters)
Grid Interval 1°
Scale 1: 333,333

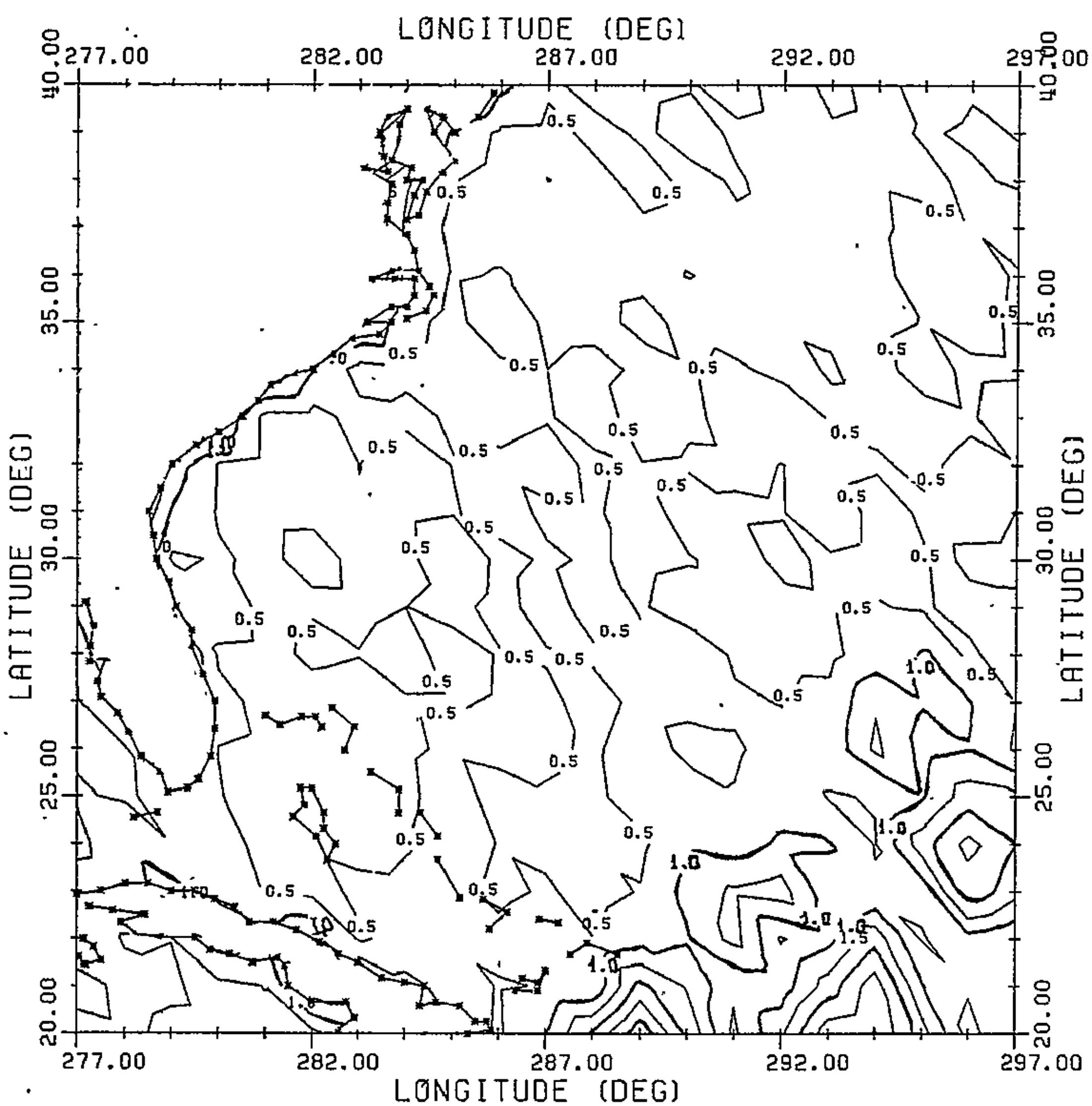

ORIGINAL PAGE IS
OF POOR QUALITY

Figure 12

Geoid Undulations - East Indian Ocean

Grid Interval 1°
Contour Interval 2 m
Scale 1: 500,000

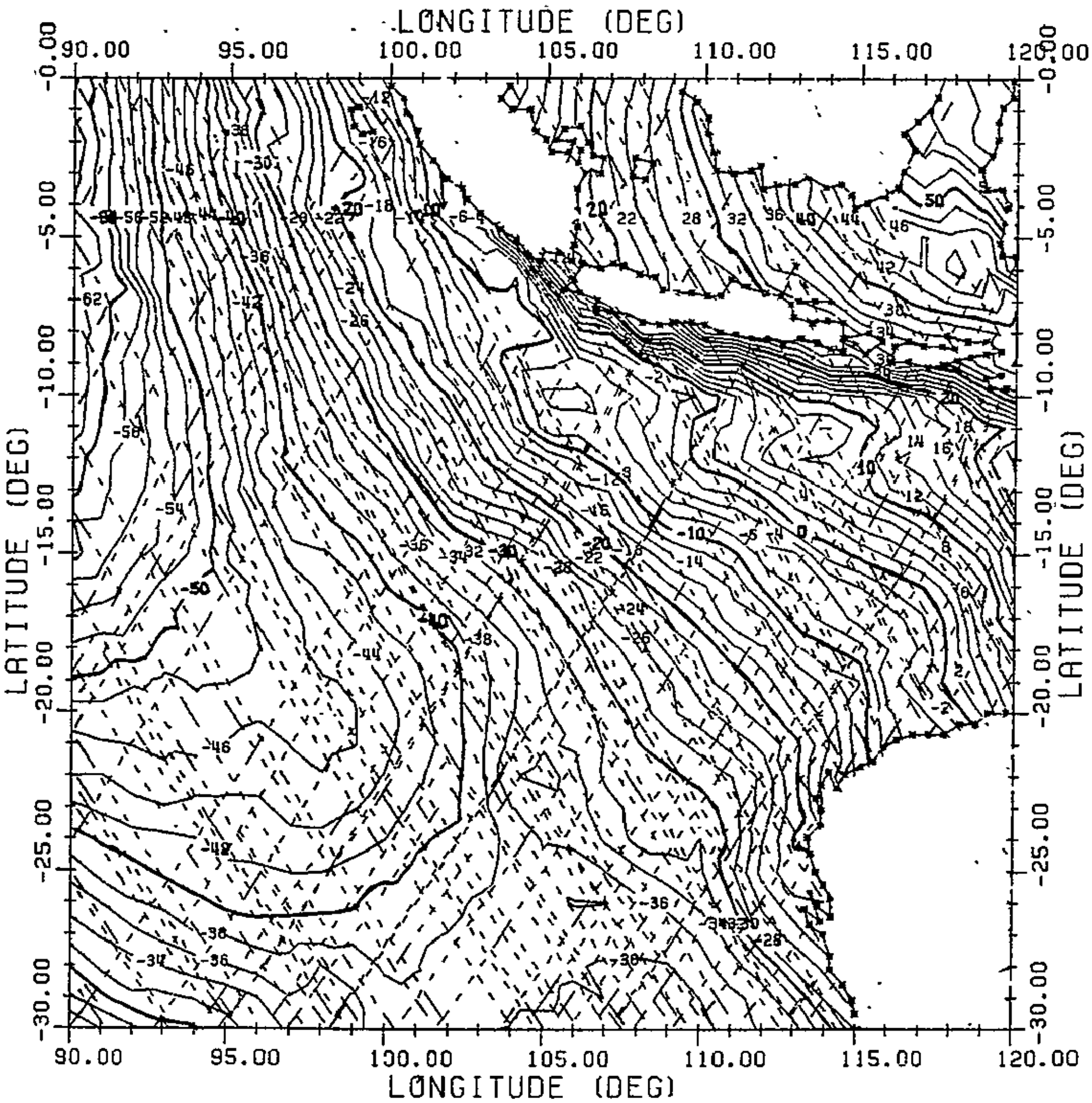

Figure 13

Precision of Prediction - East Indian Ocean

Grid Interval 1°
Contour Interval 0.5 m
Scale 1: 500,000

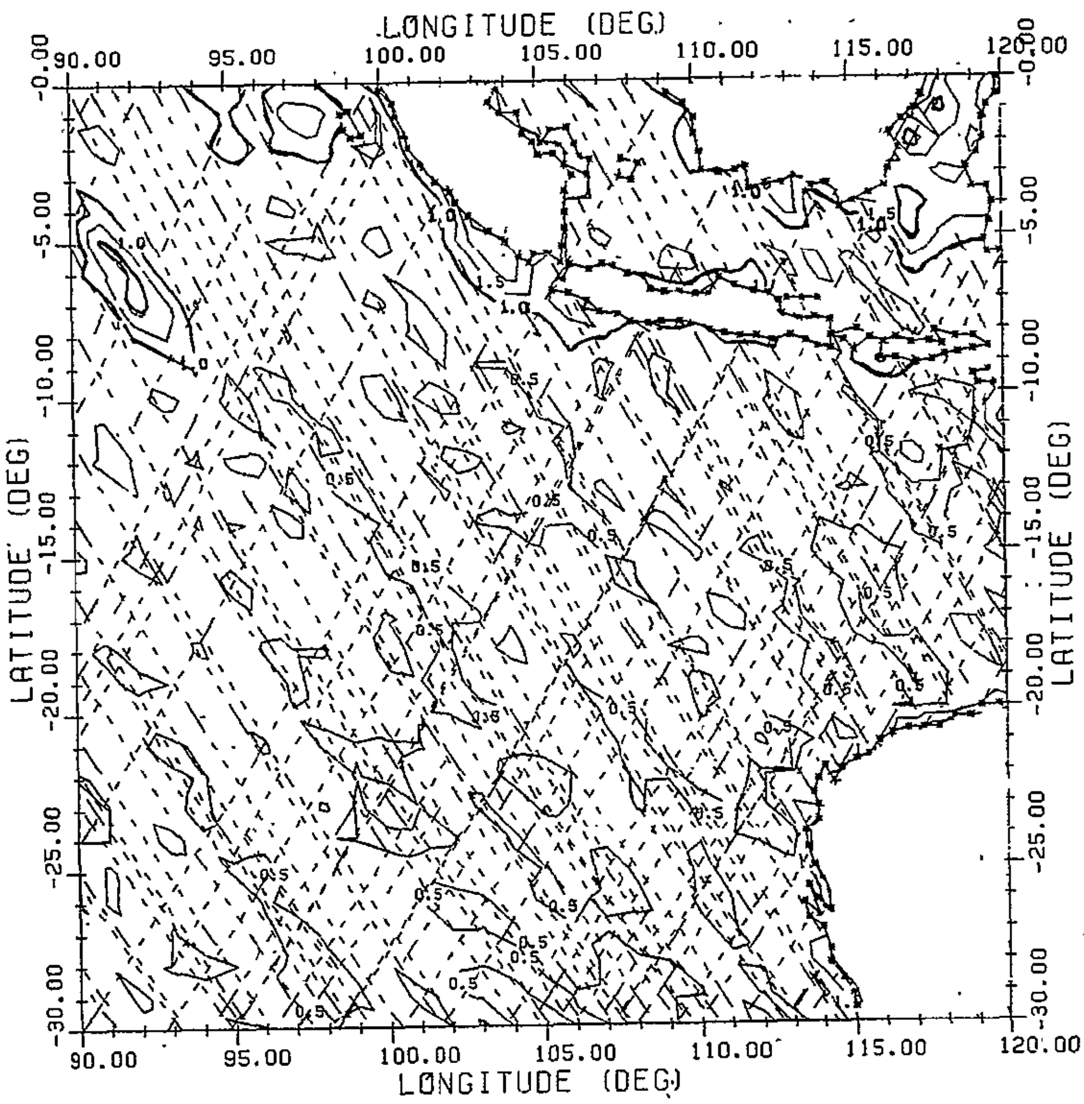

Figure 14

Geoid Undulations - Central Indian Ocean

Grid Interval 1°
Contour Interval 2 m
Scale 1: 500,000

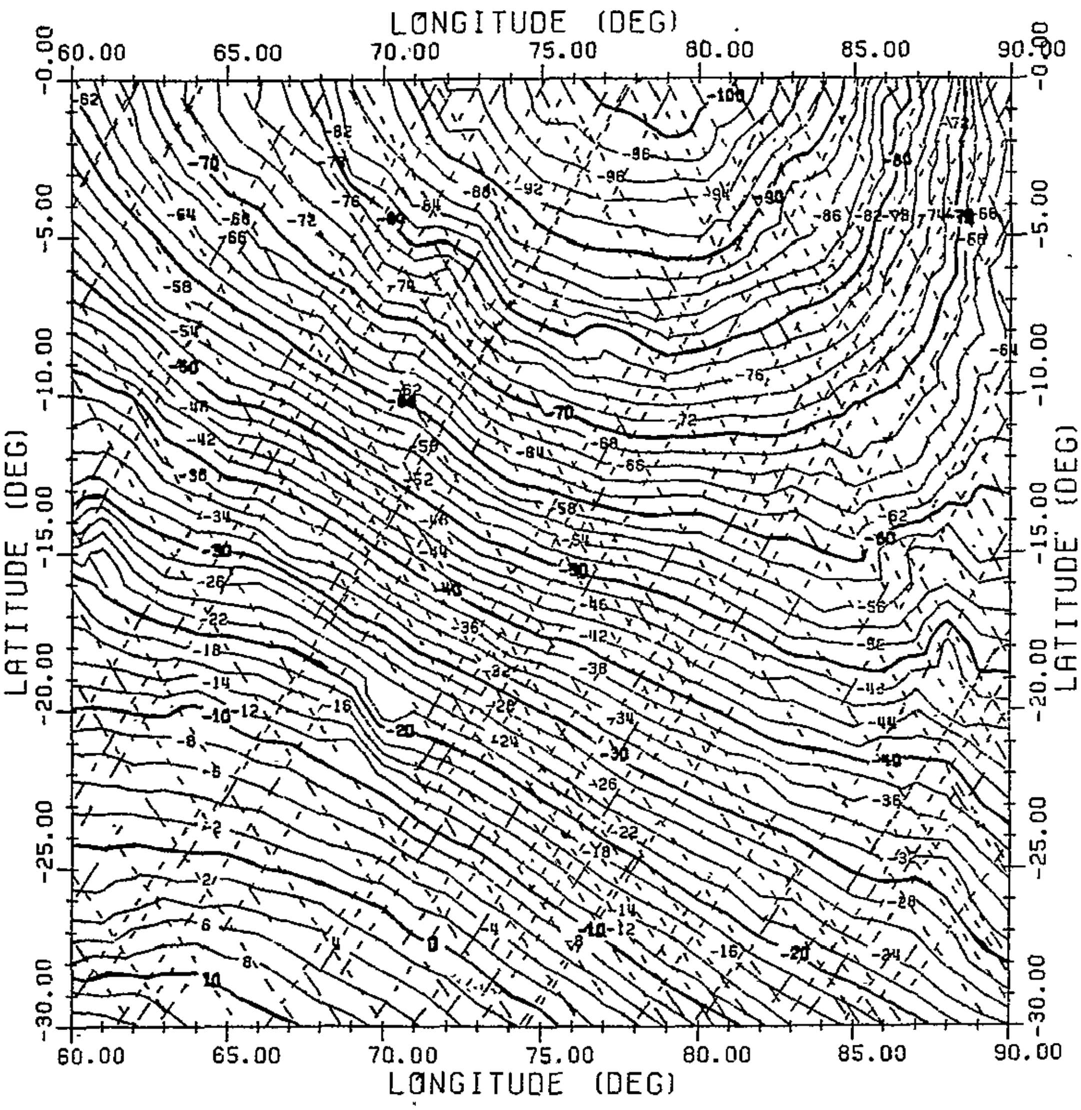

Figure 15

Precision of Prediction - Central Indian Ocean

Grid Interval 1°
Contour Interval 0.5 m
Scale 1: 500,000

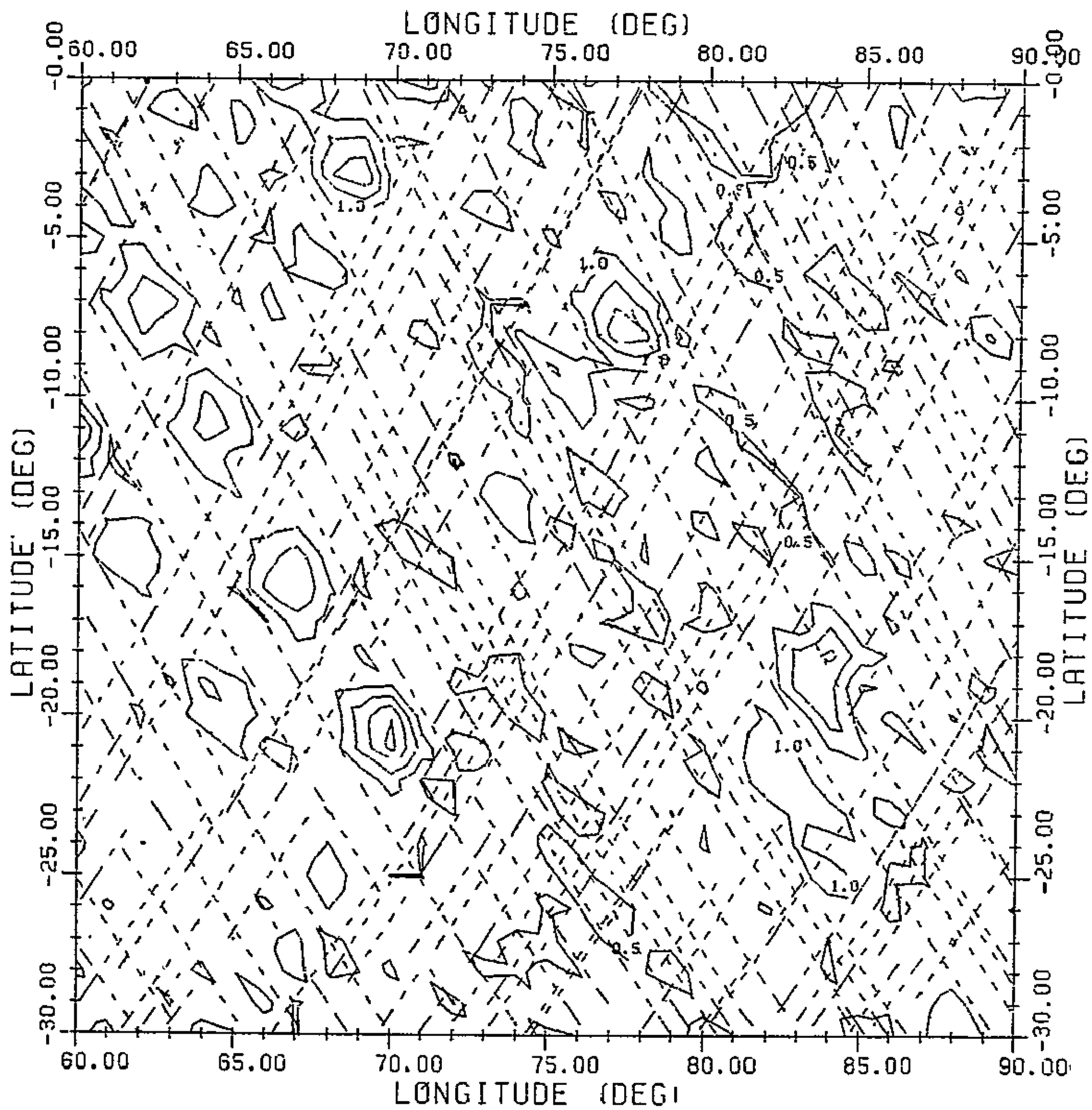

Figure 16. Geoid Undulations in the Central Indian Ocean
From Adjusted Altimeter Data.
Contour Interval: 2 meters
Grid Interval 1°
Scale 1: 500,000

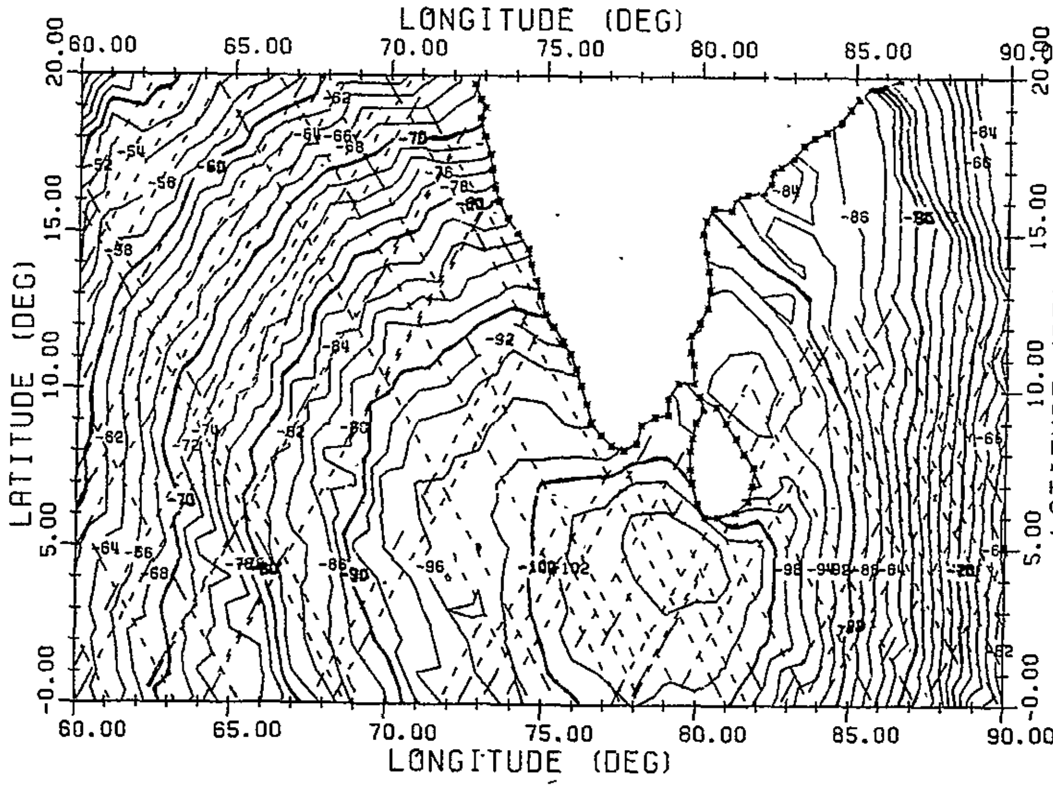

Figure 17. Geoid Undulation Accuracy in the Central Indian Ocean
From Adjusted Altimeter Data.
Contour Interval: 0.5 meter
Grid Interval 1°
Scale 1: 500,000

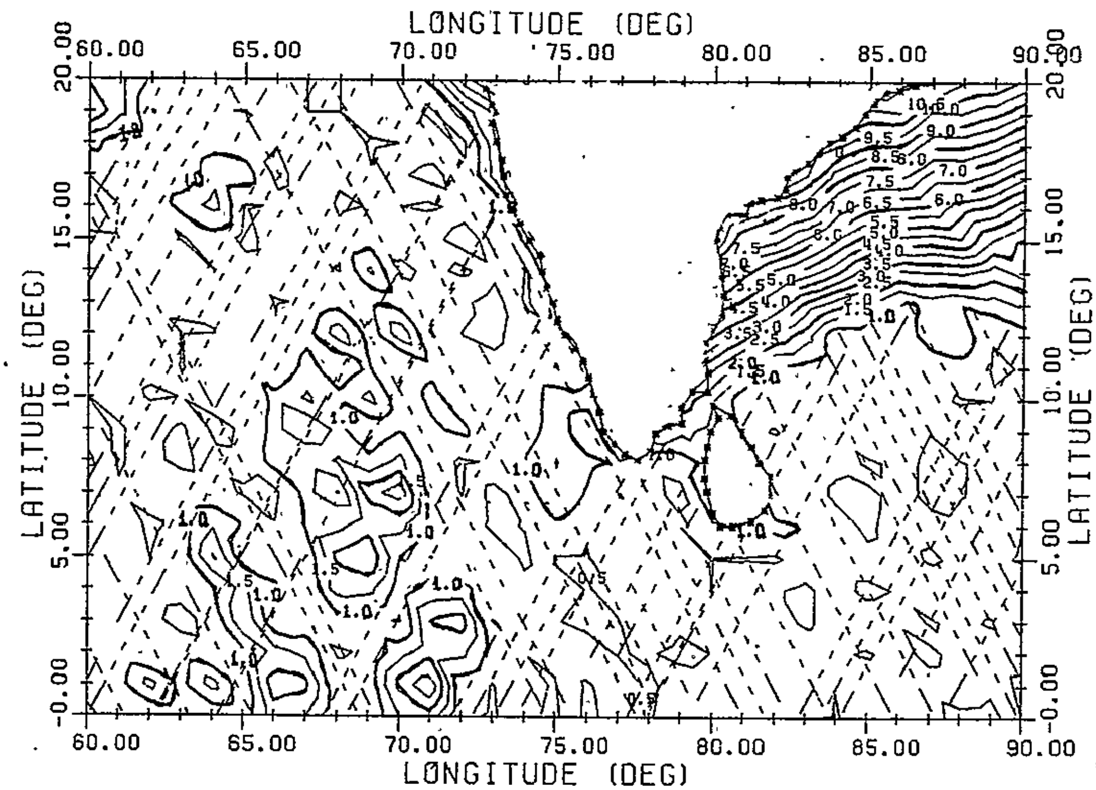

Figure 18

Geoid Undulations - S. W. U. S. Calibration Area

Grid Interval 1°
Contour Interval 2 m
Scale 1: 500,000

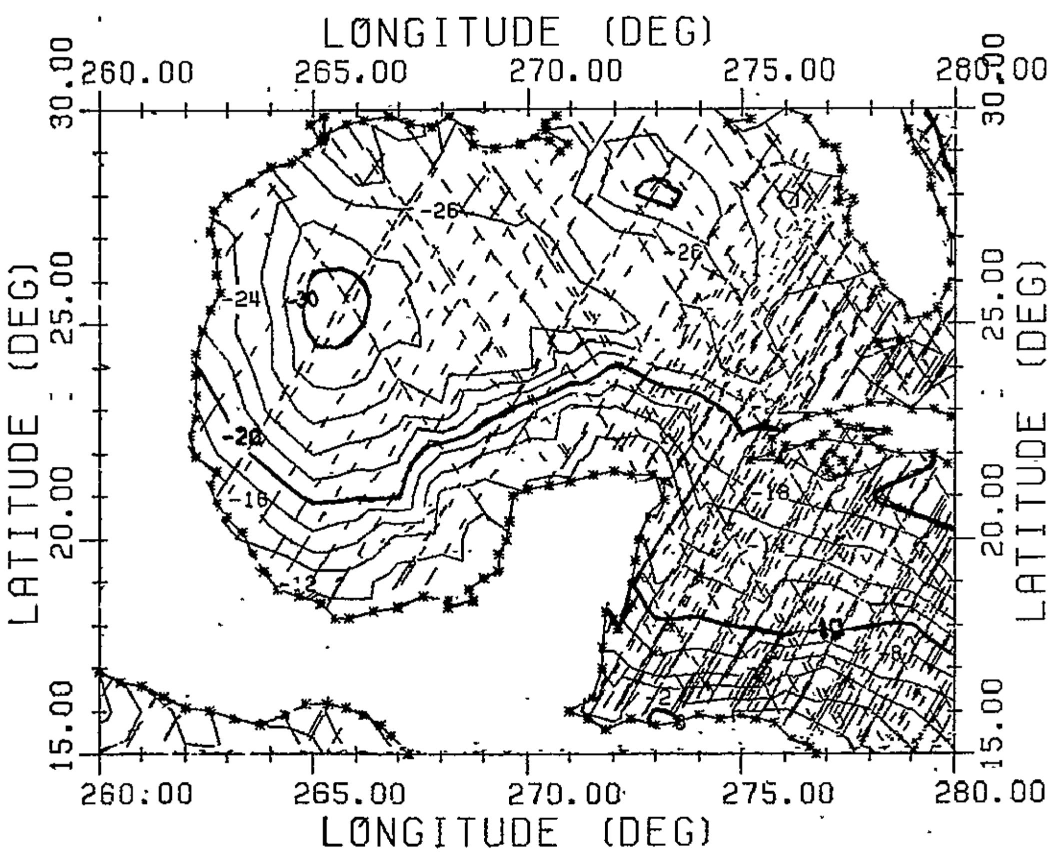

Figure 19

Precision of Prediction - S. W. U. S. Calibration Area

Grid Interval 1°
Contour Interval 0.5 m
Scale 1: 500,000

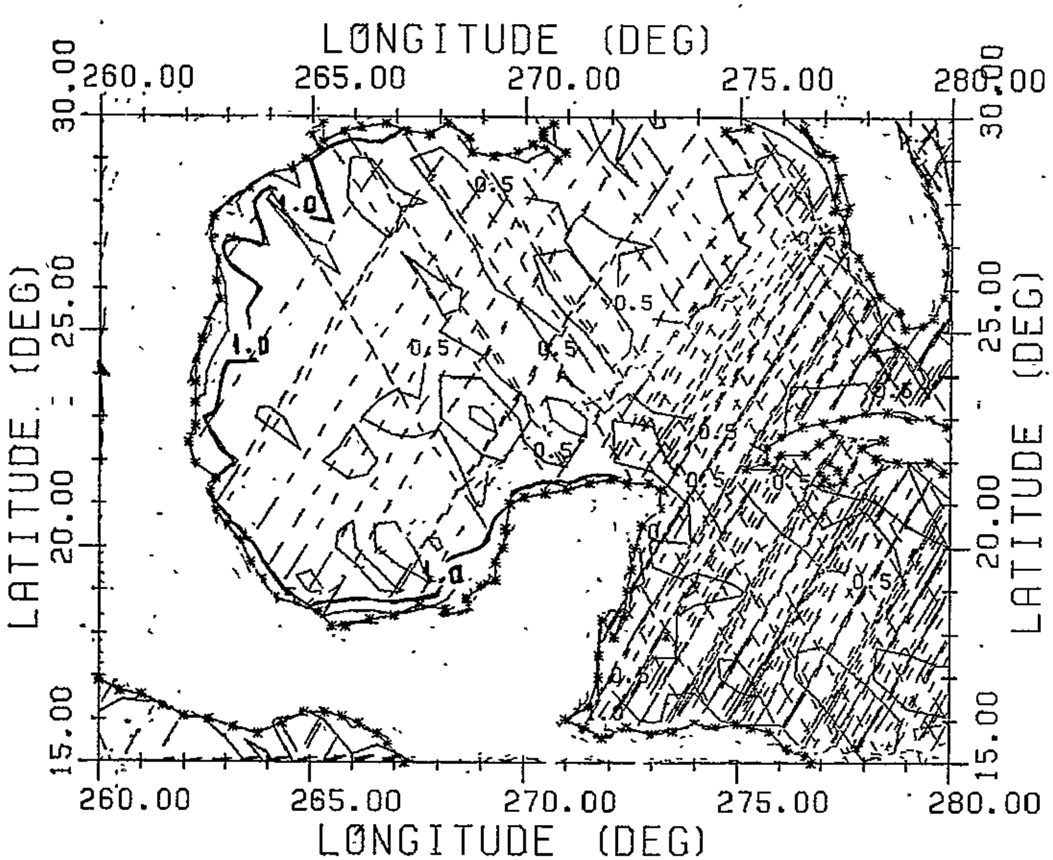

Figure 20

Geoid Undulations - S. W. Australia

Grid Interval 1°
Contour Interval 2 m
Scale 1: 500,000

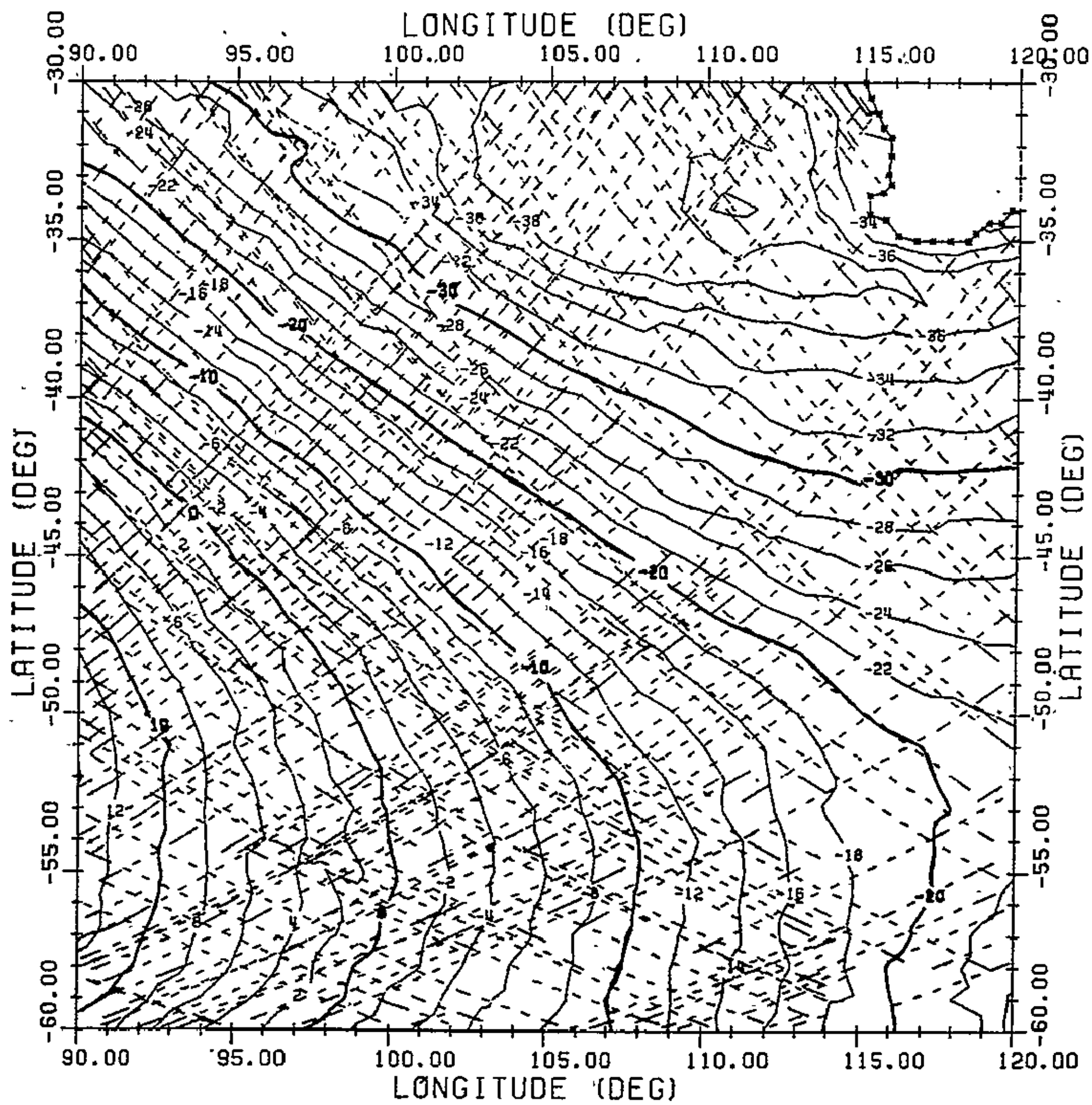

Figure 21

Precision of Prediction - S. W. Australia

Grid Interval 1°
Contour Interval 0.5 m
Scale 1: 500,000

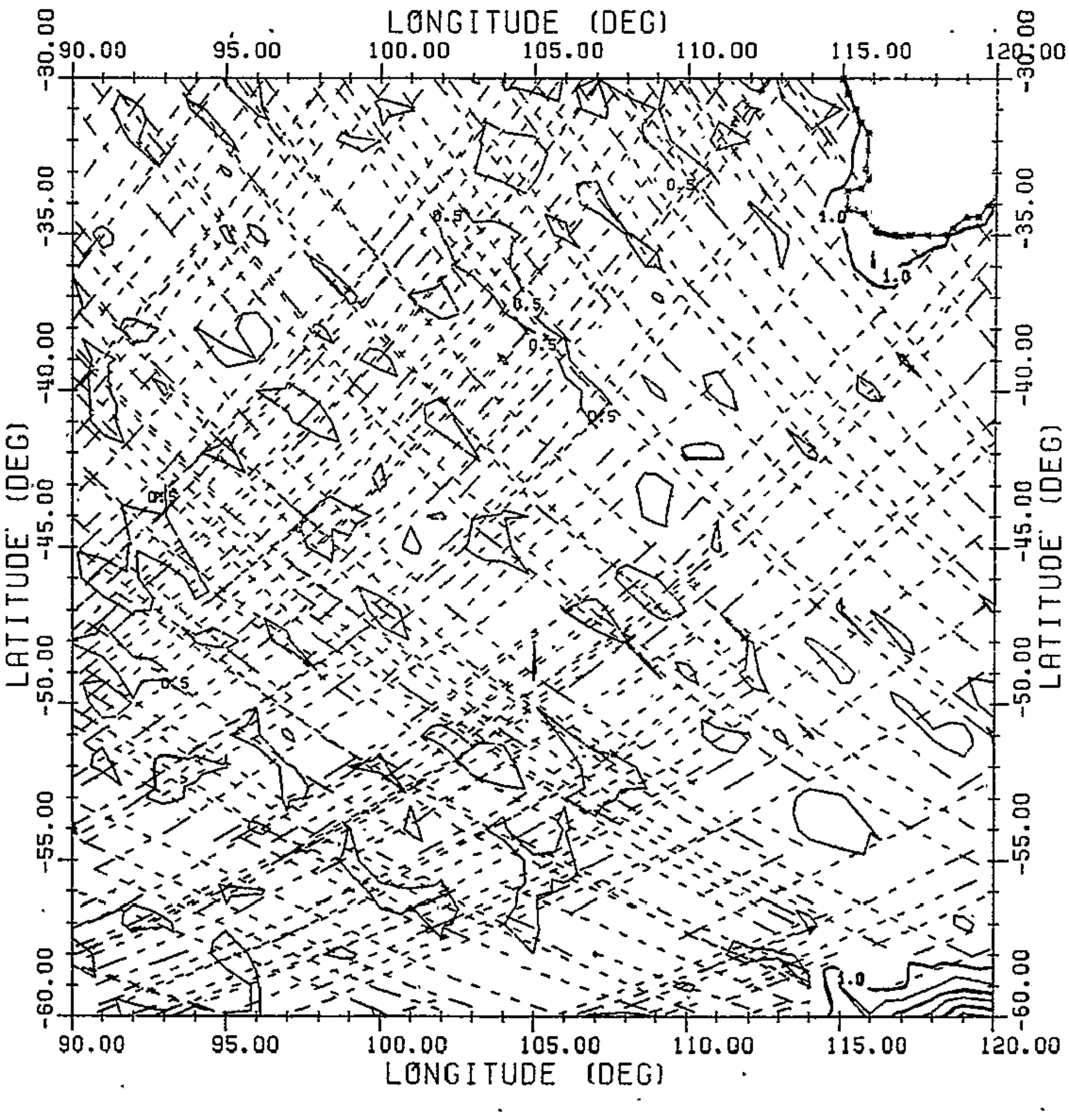

Figure 22

Geoidal Undulations - S. Central Indian Ocean

Grid Interval 1°
Contour Interval 2 m
Scale 1: 500,000

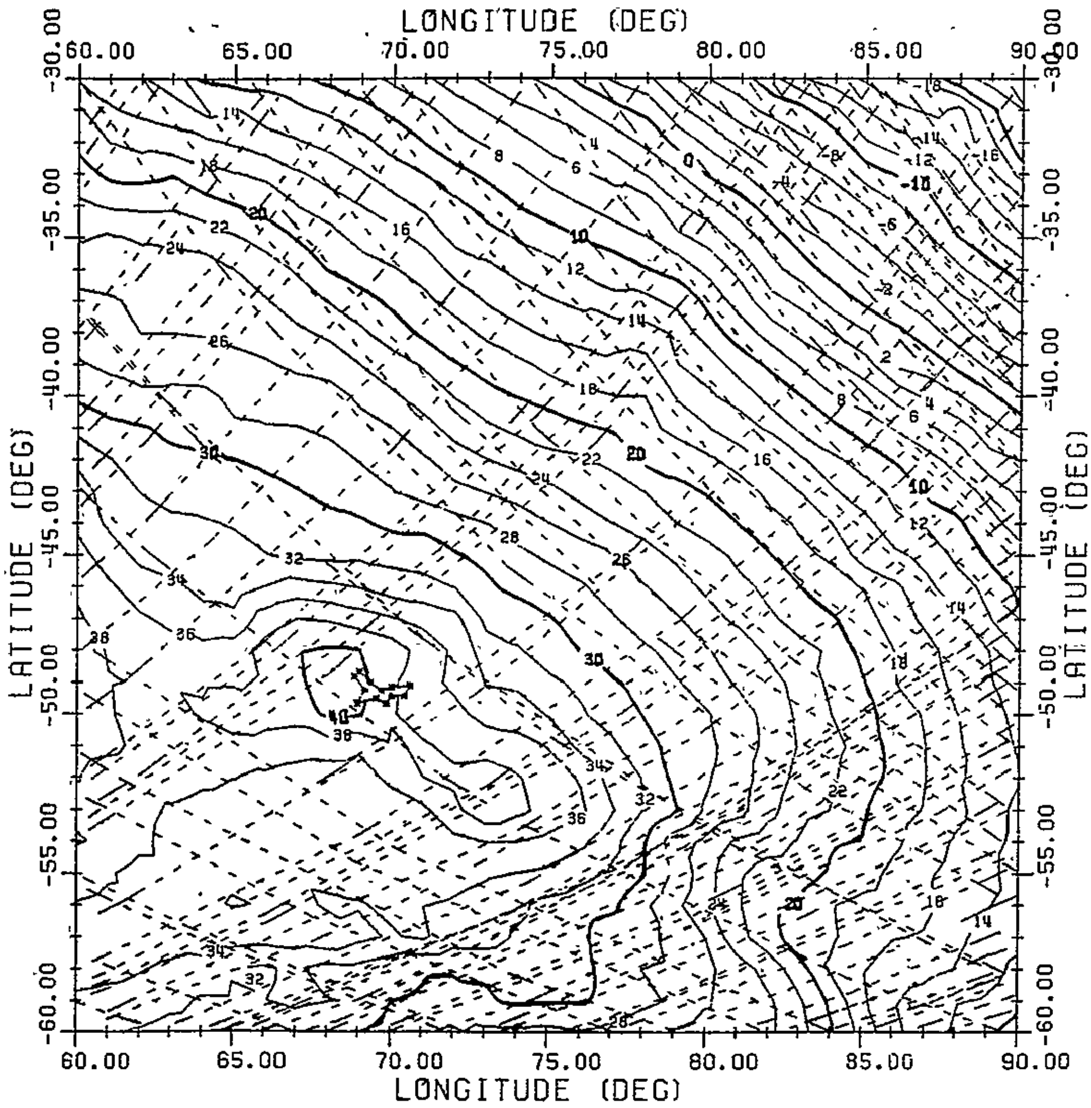

Figure 23

Precision of Prediction - S. Central Indian Ocean

Grid Interval 1°
Contour Interval 0.5 m
Scale 1: 500,000

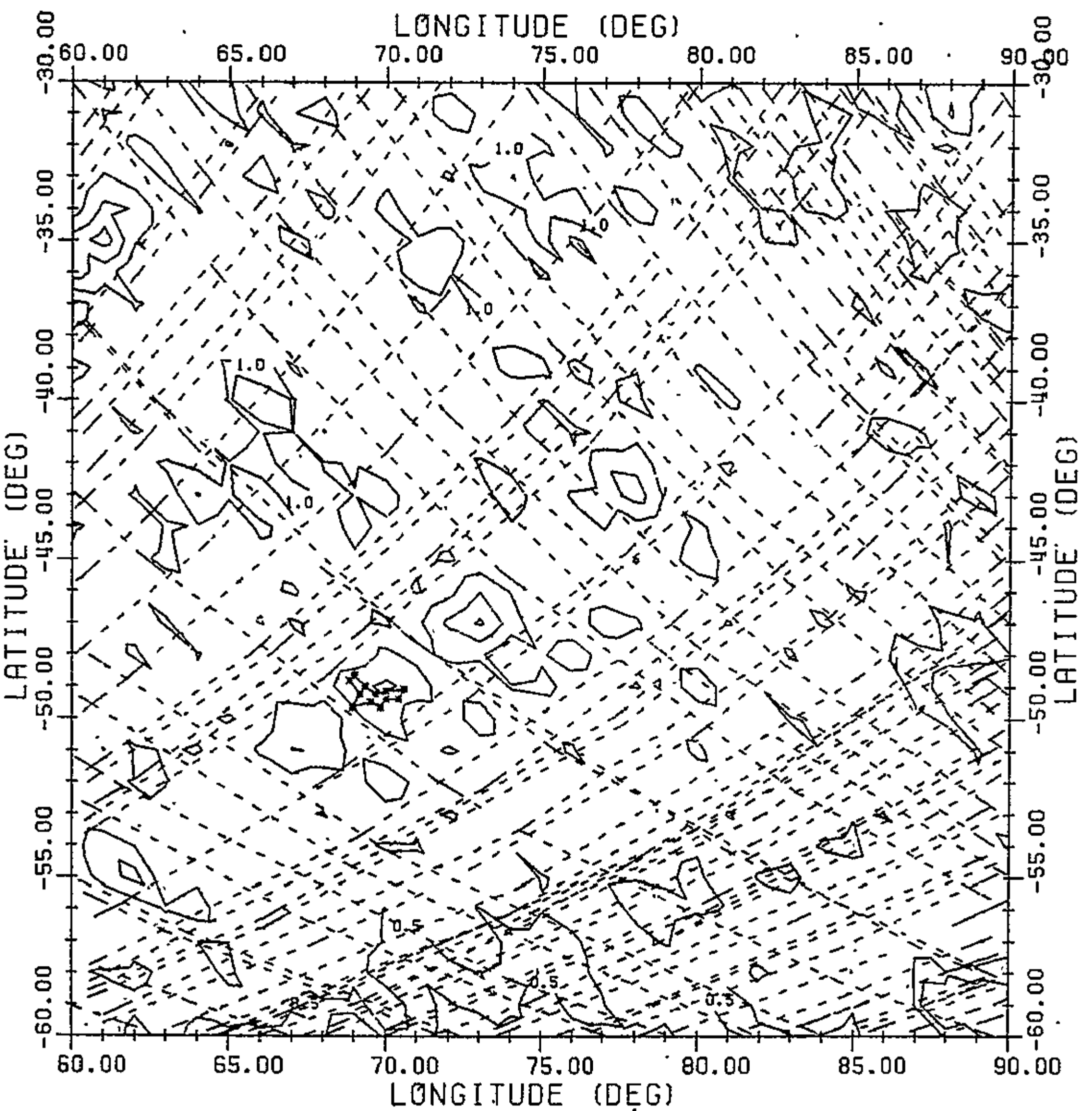

Figure 24

Geoidal Undulations - S. W. Indian Ocean

Grid Interval 1°
Contour Interval 2 m
Scale 1: 500,000

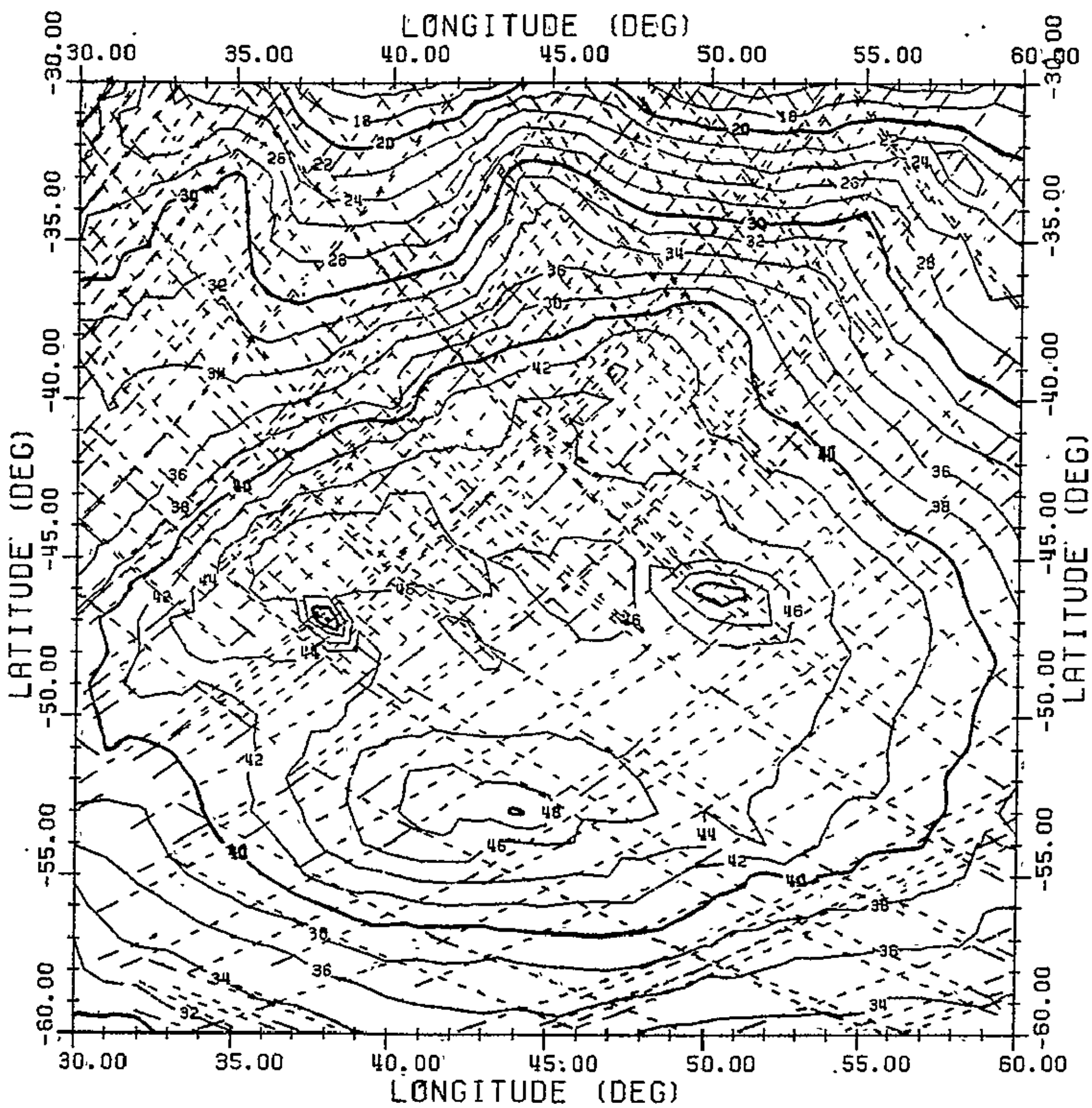

Figure 25

Precision of Prediction - S. W. Indian Ocean

Grid Interval 1°
Contour Interval 0.5 m
Scale 1: 500,000

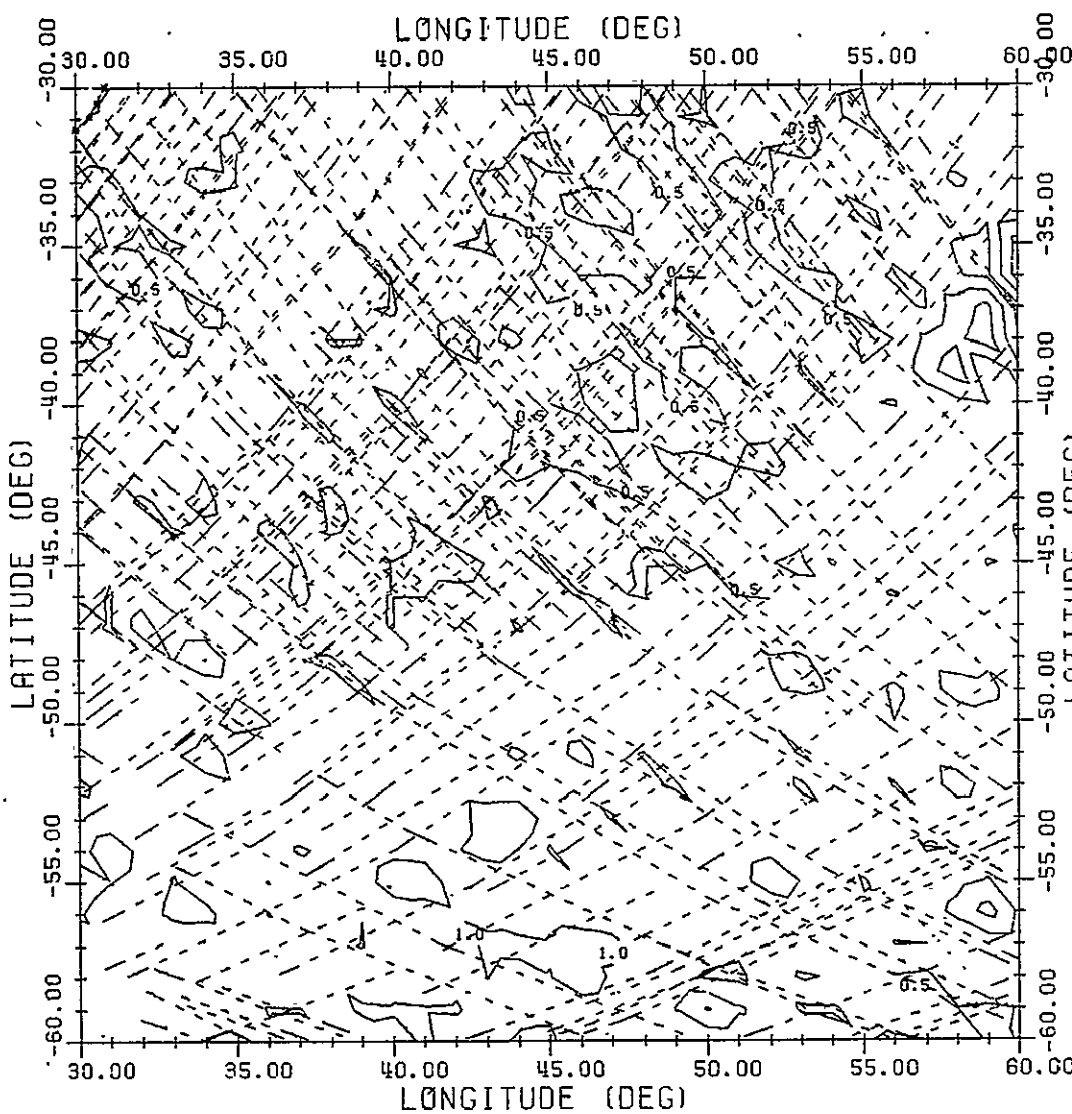

ORIGINAL PAGE IS
OF POOR QUALITY

Figure 26

Geoidal Undulations - East Africa

Grid Interval 1°
Contour Interval 2 m
Scale 1: 500,000

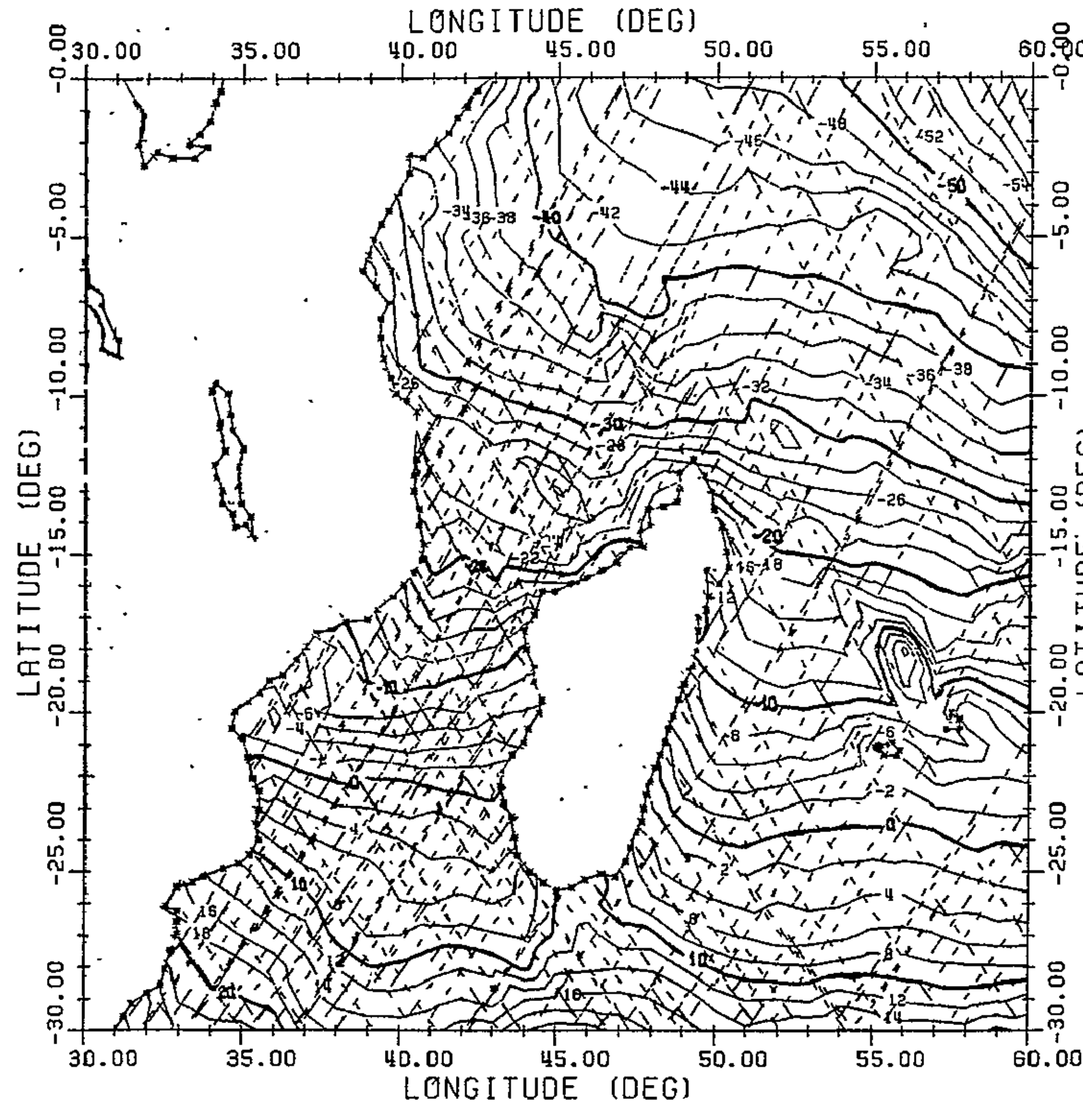

Figure 27

Precision of Prediction - East Africa

Grid Interval 1°
Contour Interval 0.5 m
Scale 1: 500,000

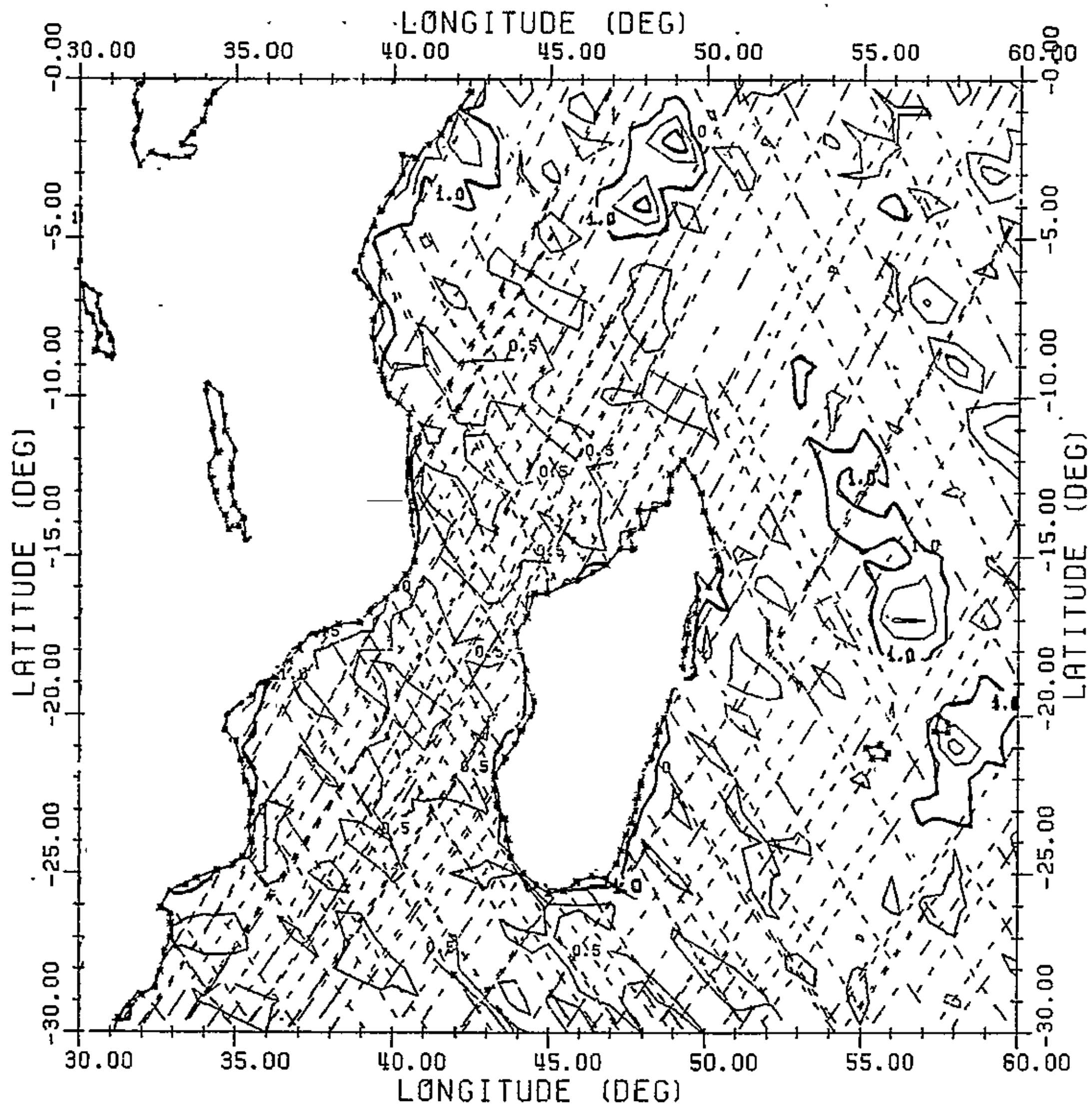

Figure 28

Geoidal Undulations - Southern Australia

Grid Interval 1°
Contour Interval 2 m .
Scale 1: 500,000

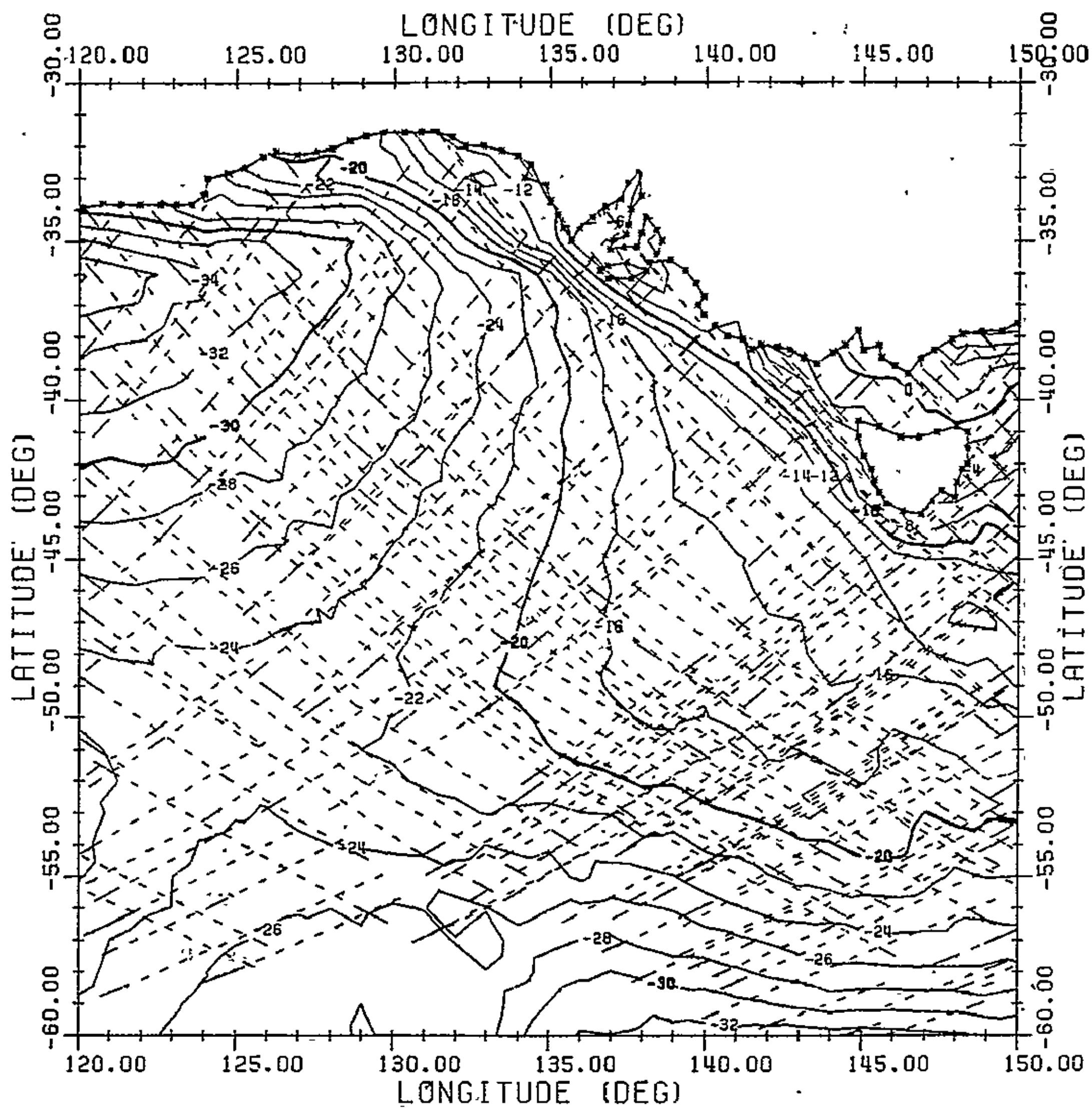

Figure 29

Precision of Prediction - Southern Australia

Grid Interval 1°
Contour Interval 0.5 m
Scale 1: 500,000

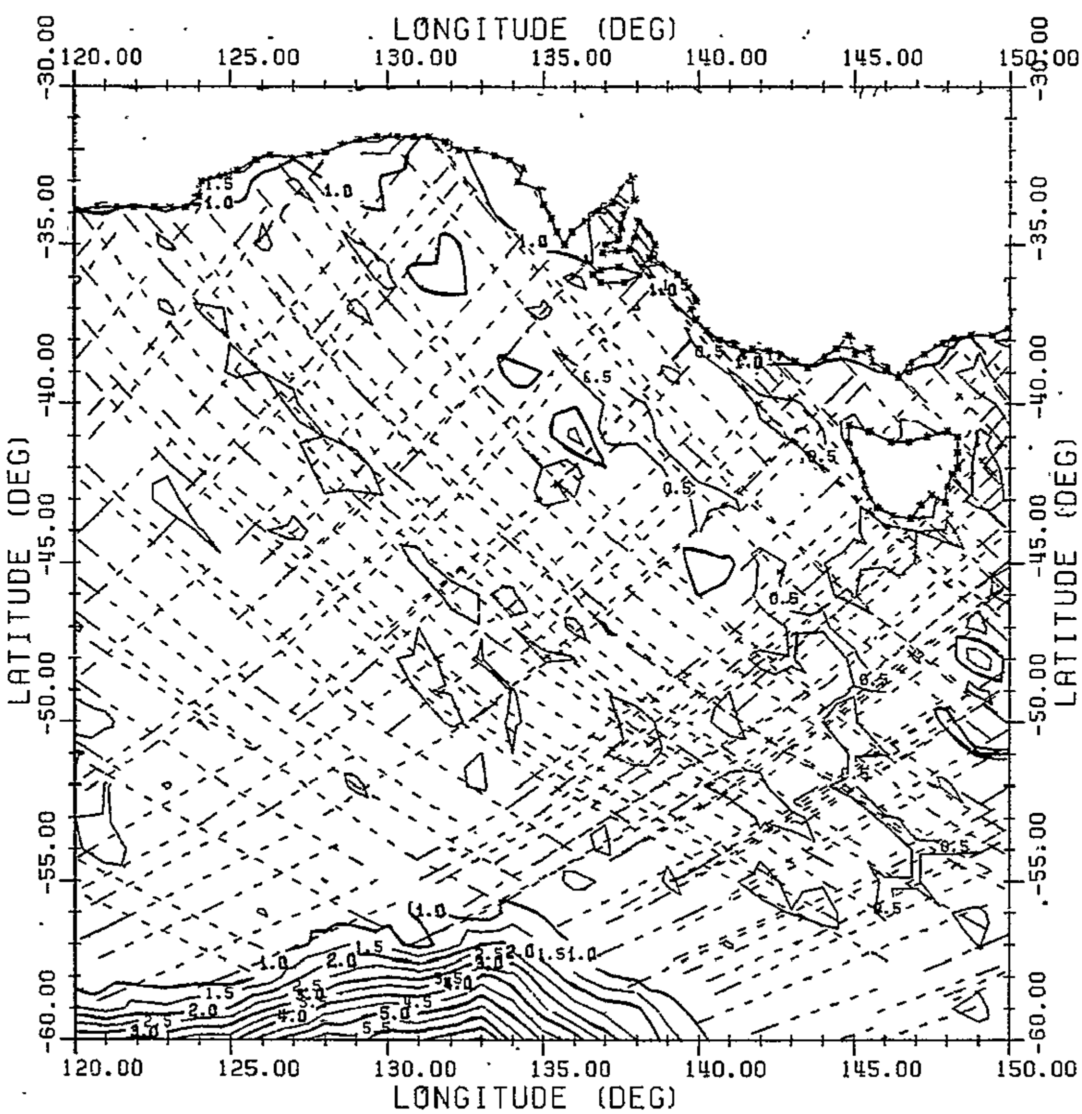

Figure 30

Geoidal Undulations - Tasman Sea

Grid Interval 1°
Contour Interval 2 m
Scale 1: 500,000

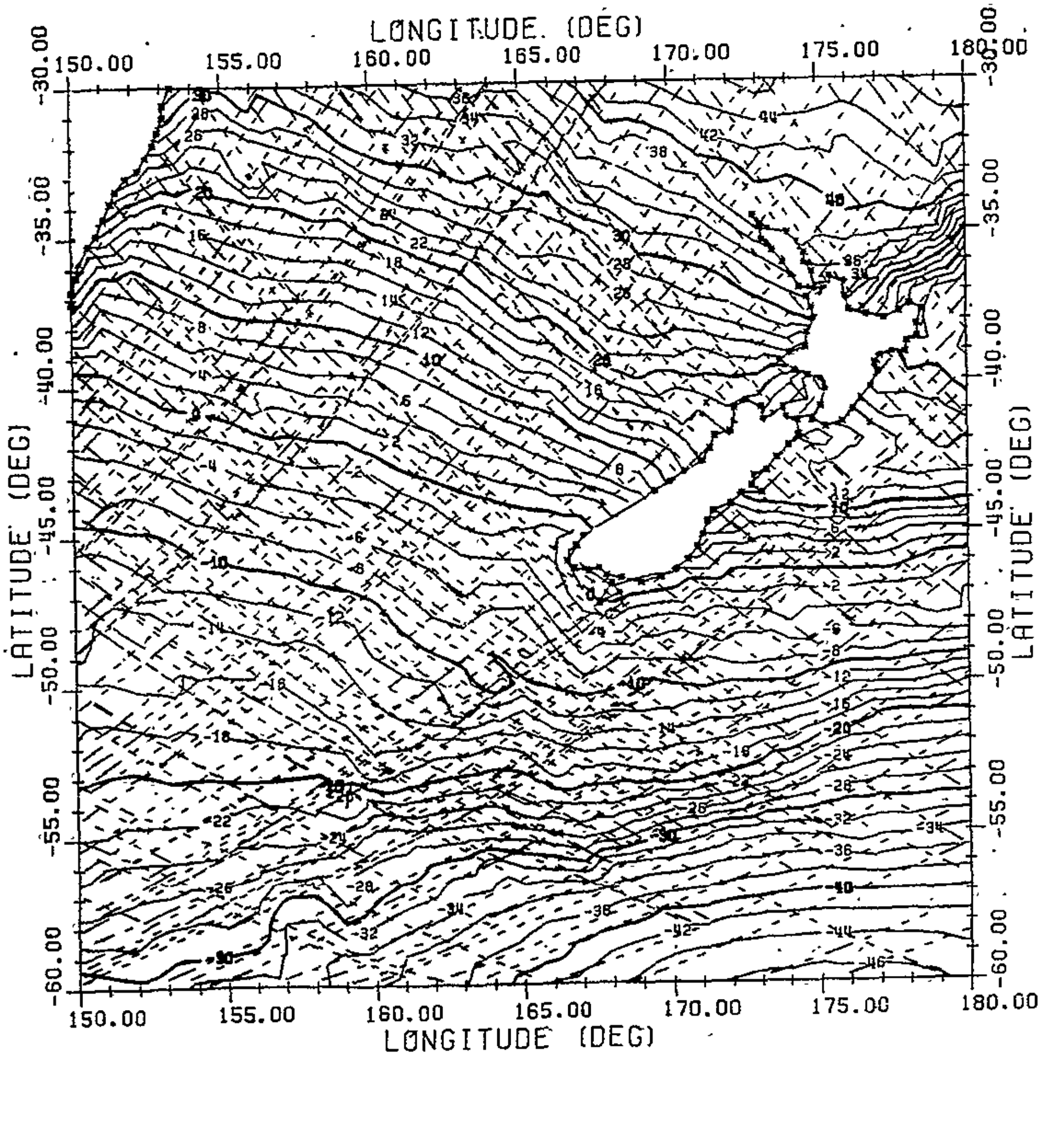

Figure 31

Precision of Prediction - Tasman Sea

Grid Interval 1°
Contour Interval 0.5 m
Scale 1: 500,000

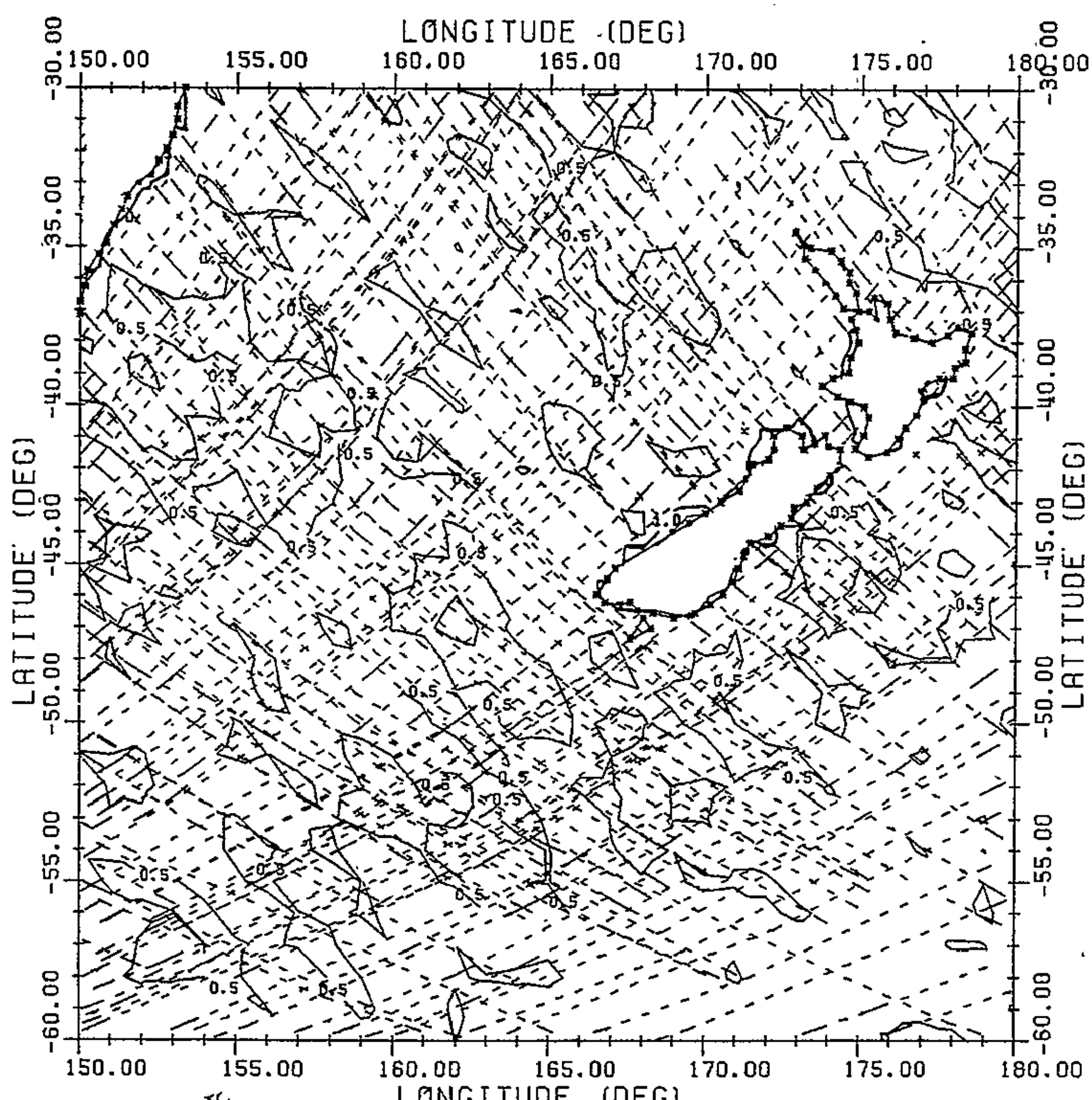

Figure 32

Geoidal Undulations - N. E. Australia

Grid Interval 1°
Contour Interval 2 m
Scale 1: 500,000

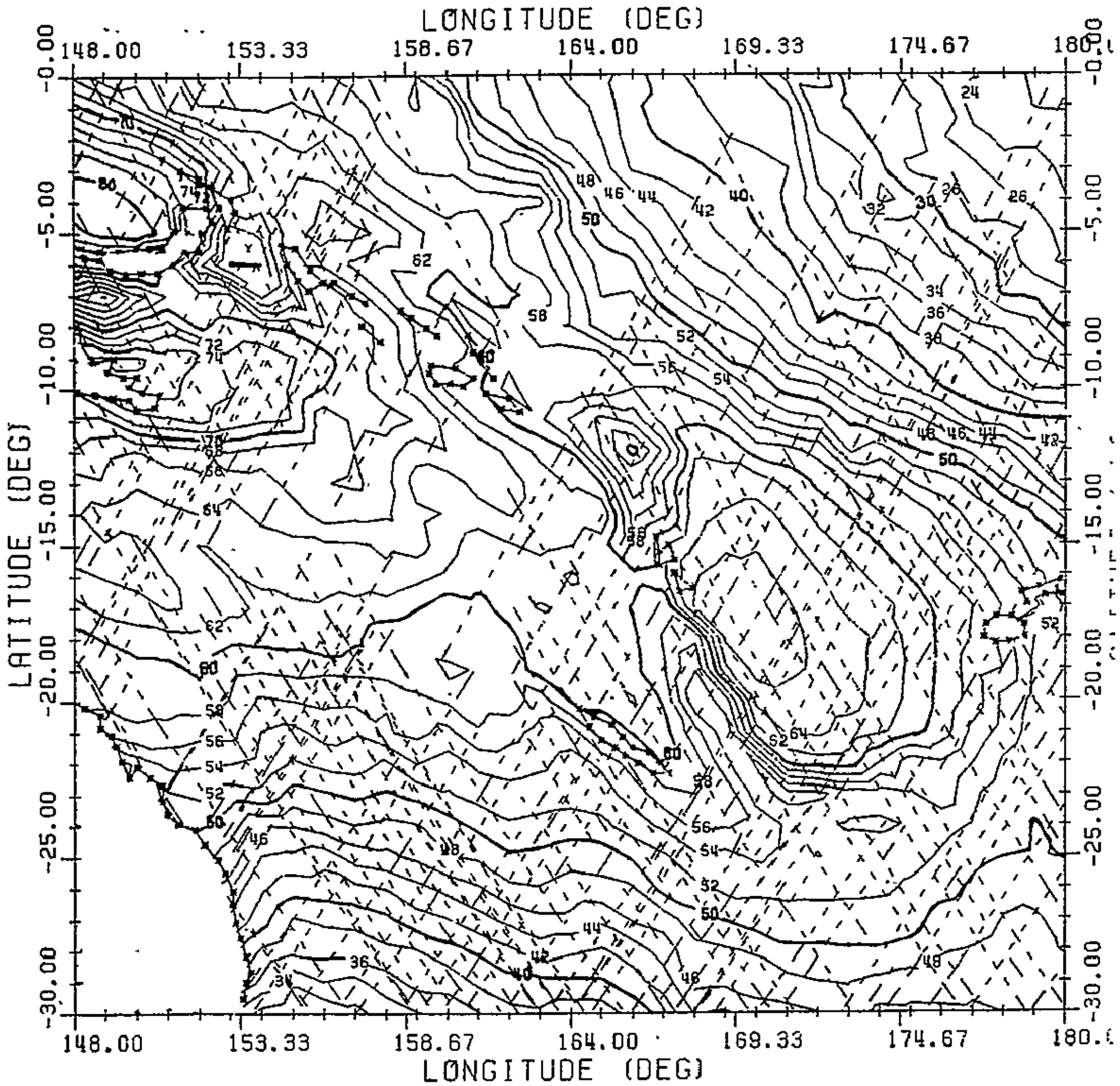

Figure 33

Precision of Prediction - N. E. Australia

Grid Interval 1°
Contour Interval 0.5 m
Scale 1: 500,000

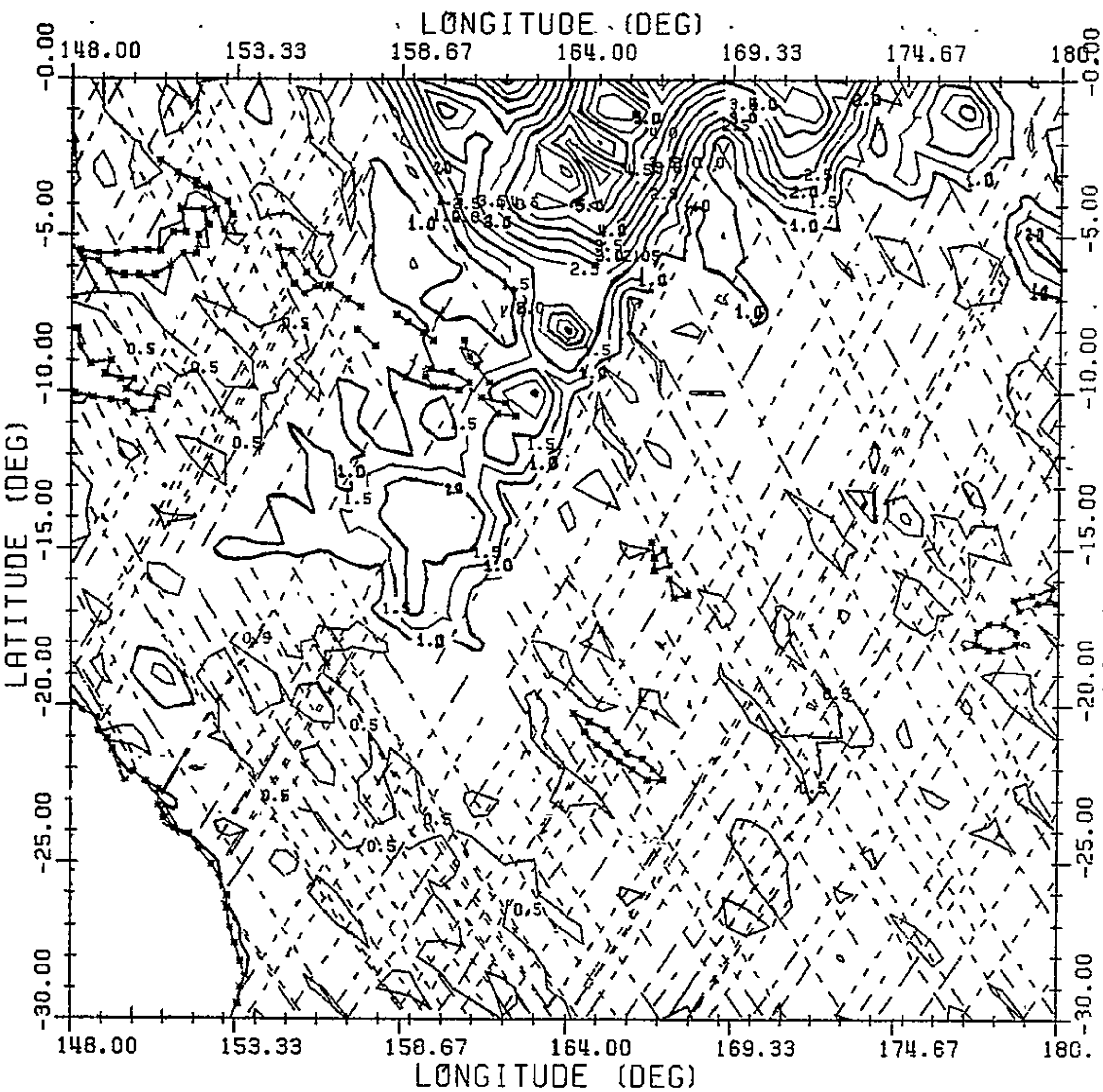

Figure 34

Geoidal Undulations - Mid Central Pacific

Grid Interval 1°
Contour Interval 2 m
Scale 1: 500,000

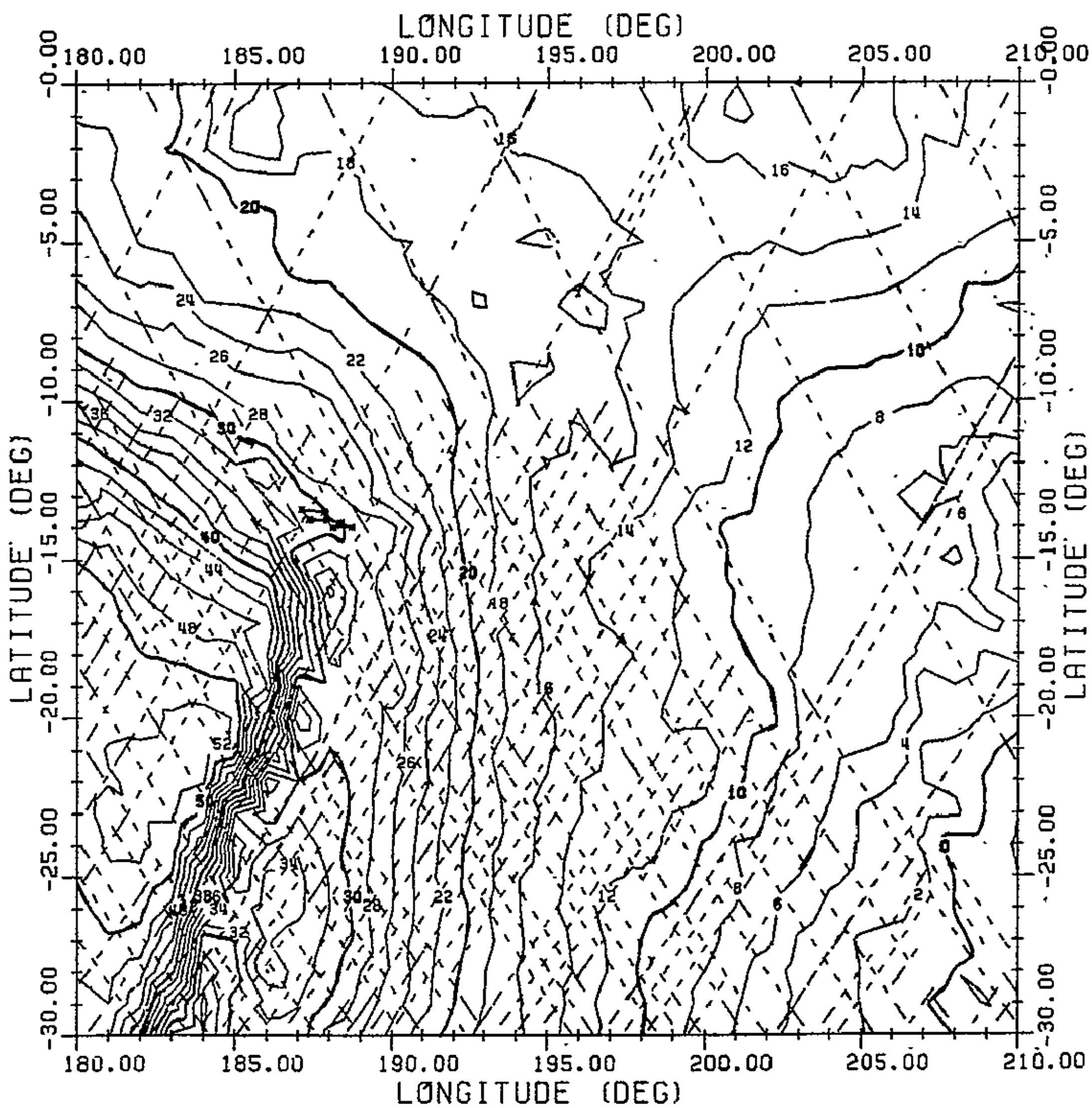

Figure 35

Precision of Prediction - Mid Central Pacific

Grid Interval 1°
Contour Interval 0.5 m
Scale 1: 500,000

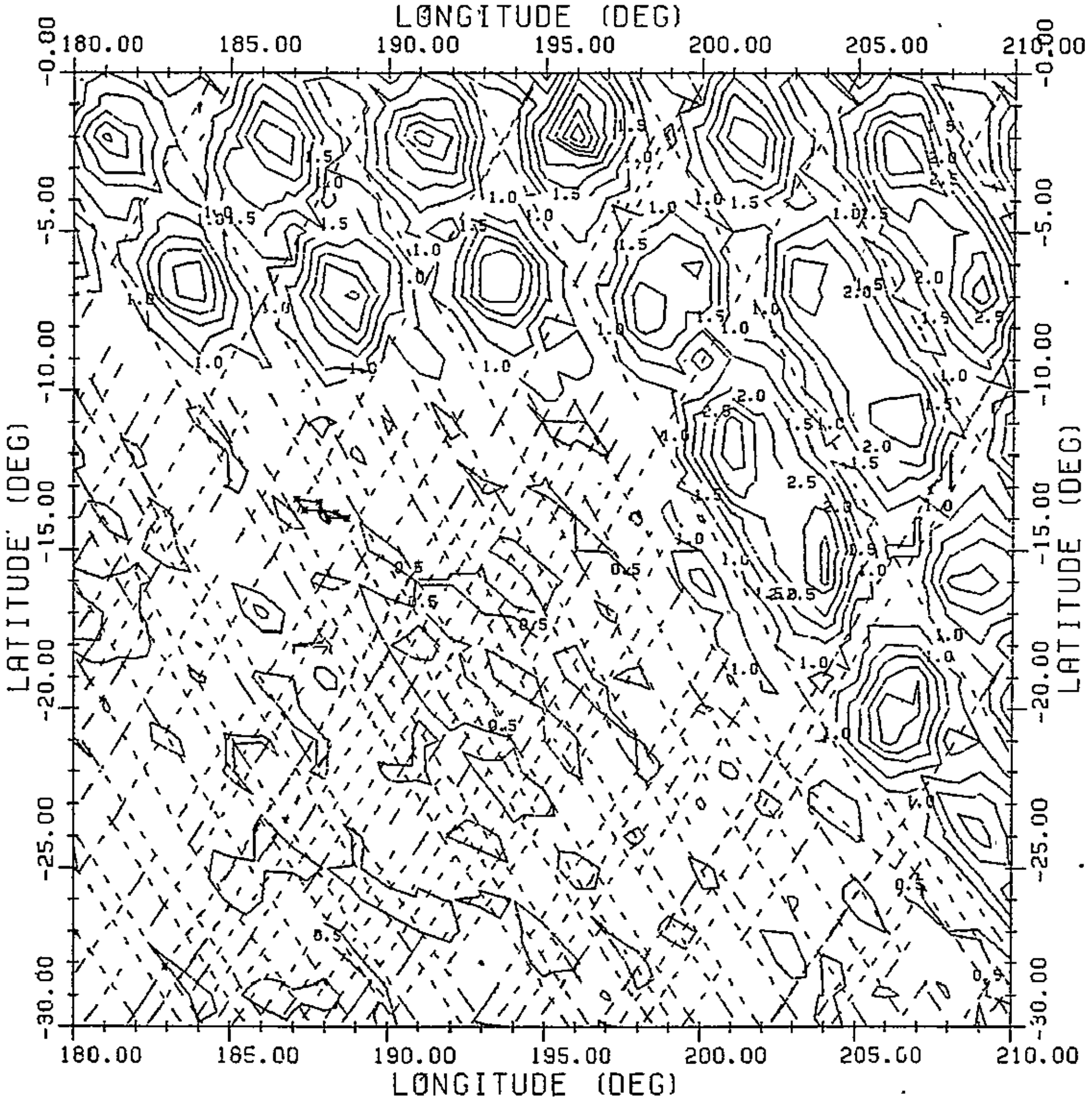

Figure 36

Geoidal Undulations - S. Central Pacific

Grid Interval 1°
Contour Interval 2 m
Scale 1: 500,000

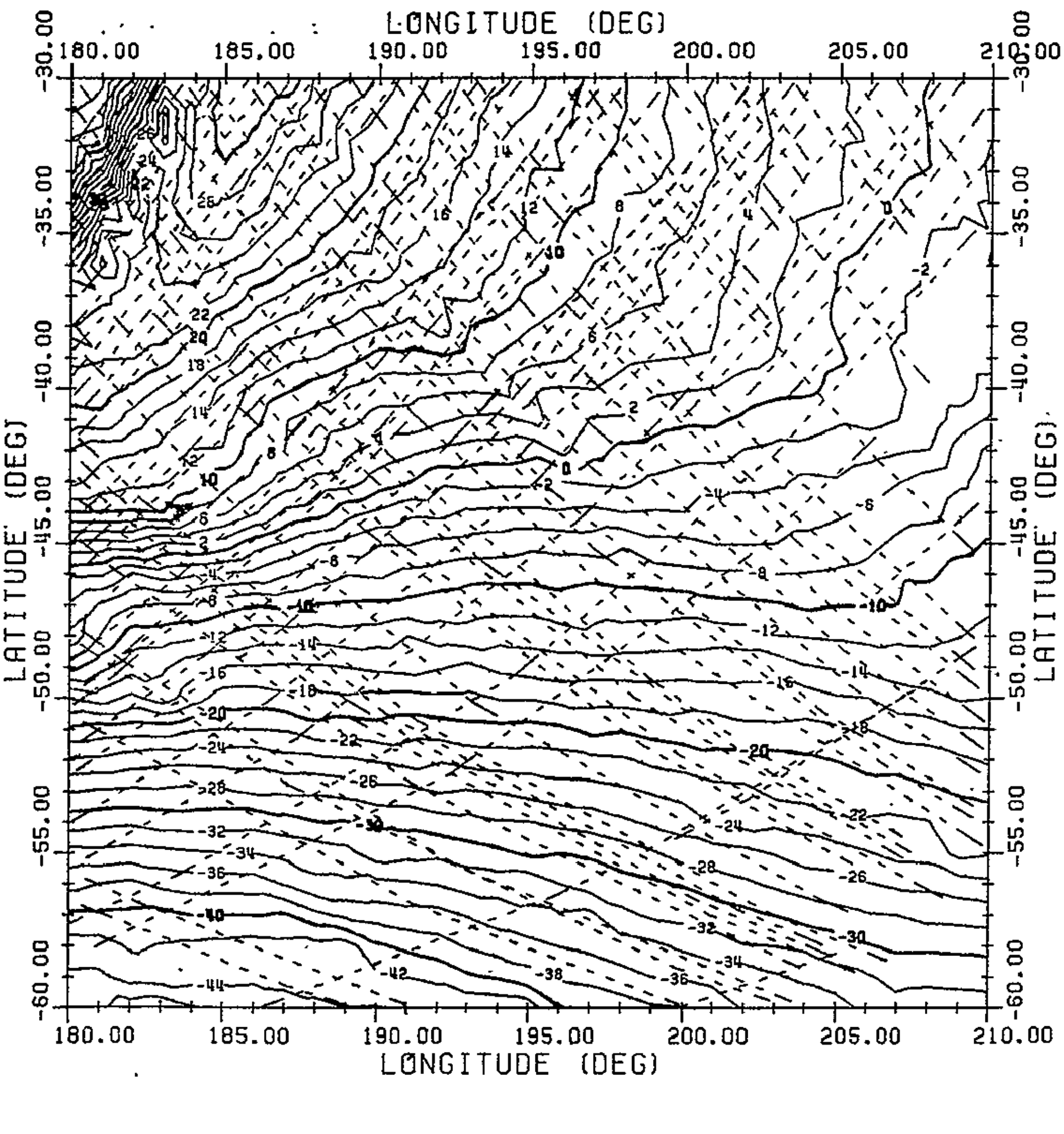

Figure 37

Precision of Prediction - S. Central Pacific

Grid Interval 1°
Contour Interval 0.5 m
Scale 1: 500,000

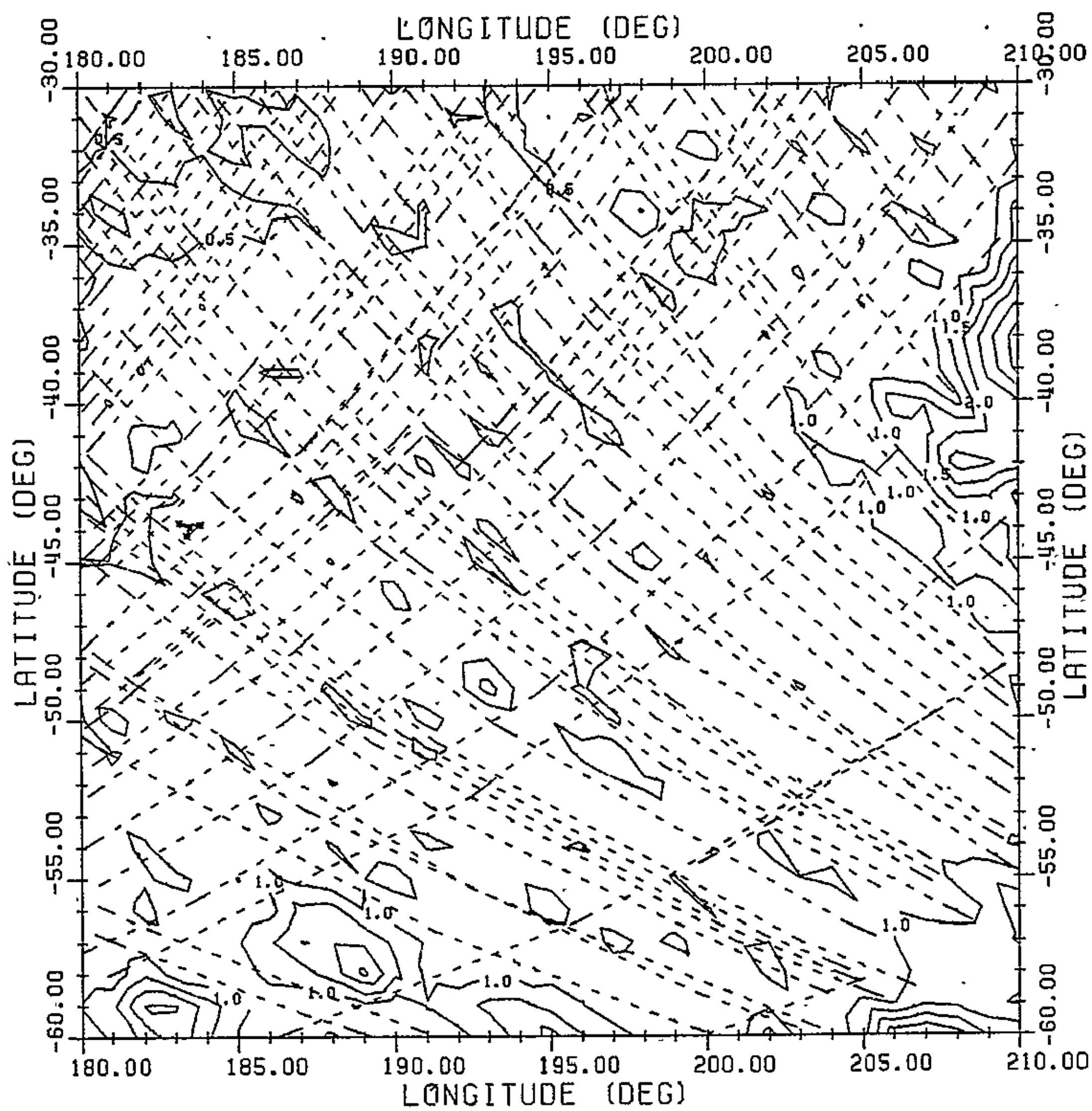

Figure 38

Geoidal Undulations - S. W. Atlantic

Grid Interval 1°
Contour Interval 2 m
Scale 1: 500,000

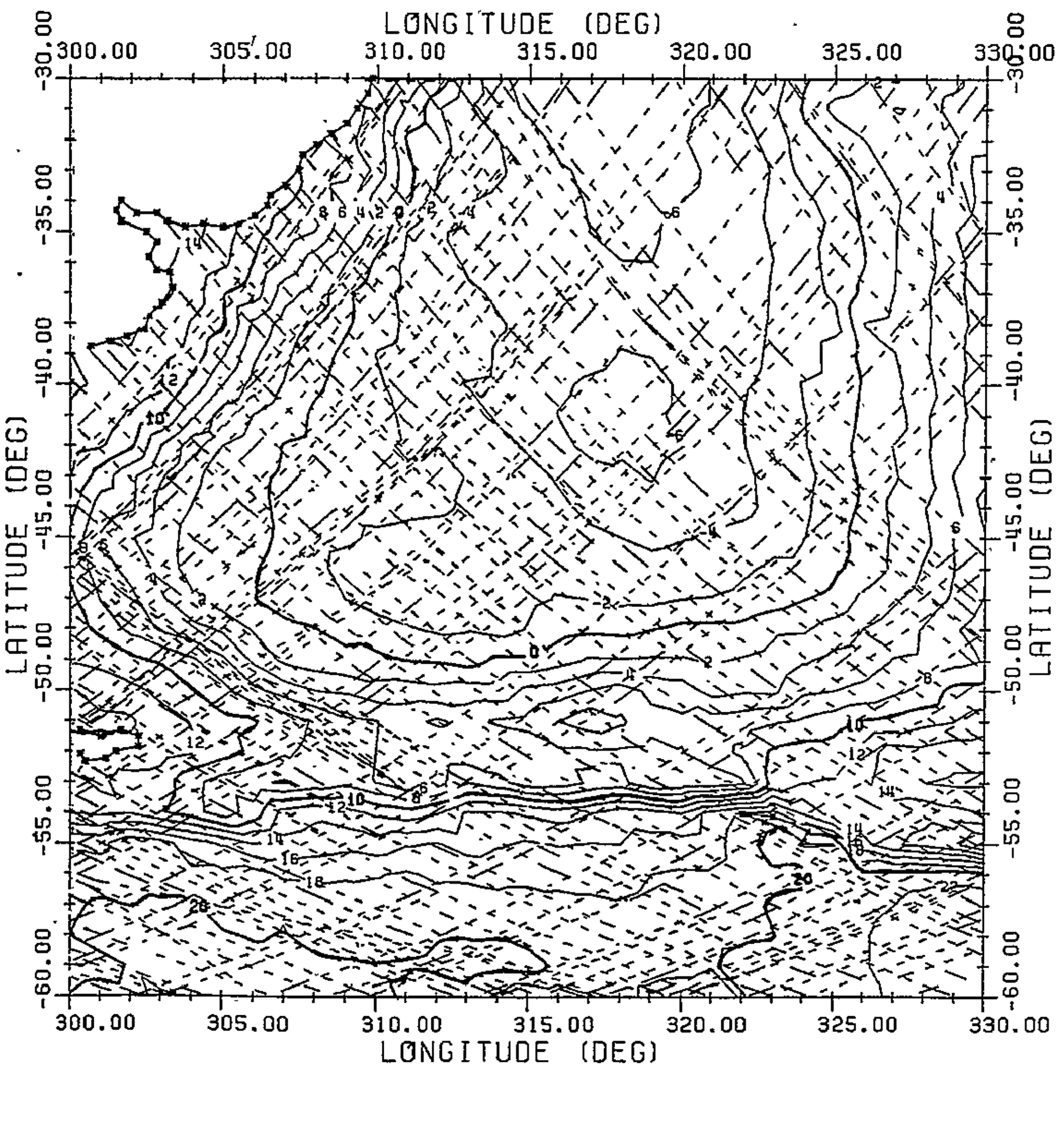

Figure 39

Precision of Prediction - S. W. Atlantic

Grid Interval 1°
Contour Interval 0.5 m
Scale 1: 500,000

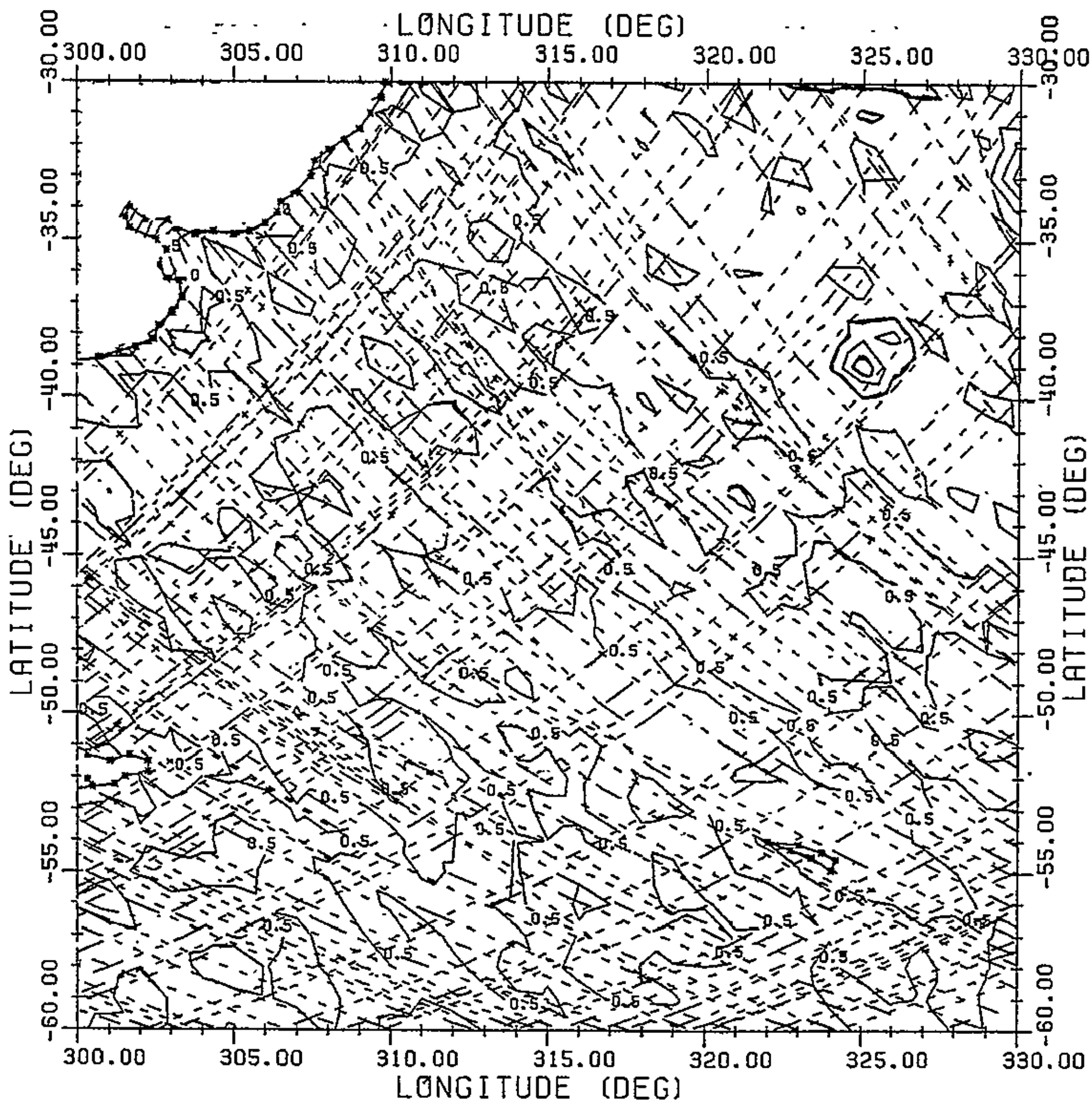

Figure 40

Geoidal Undulations - South America

Grid Interval 1°
Contour Interval 2 m
Scale 1: 500,000

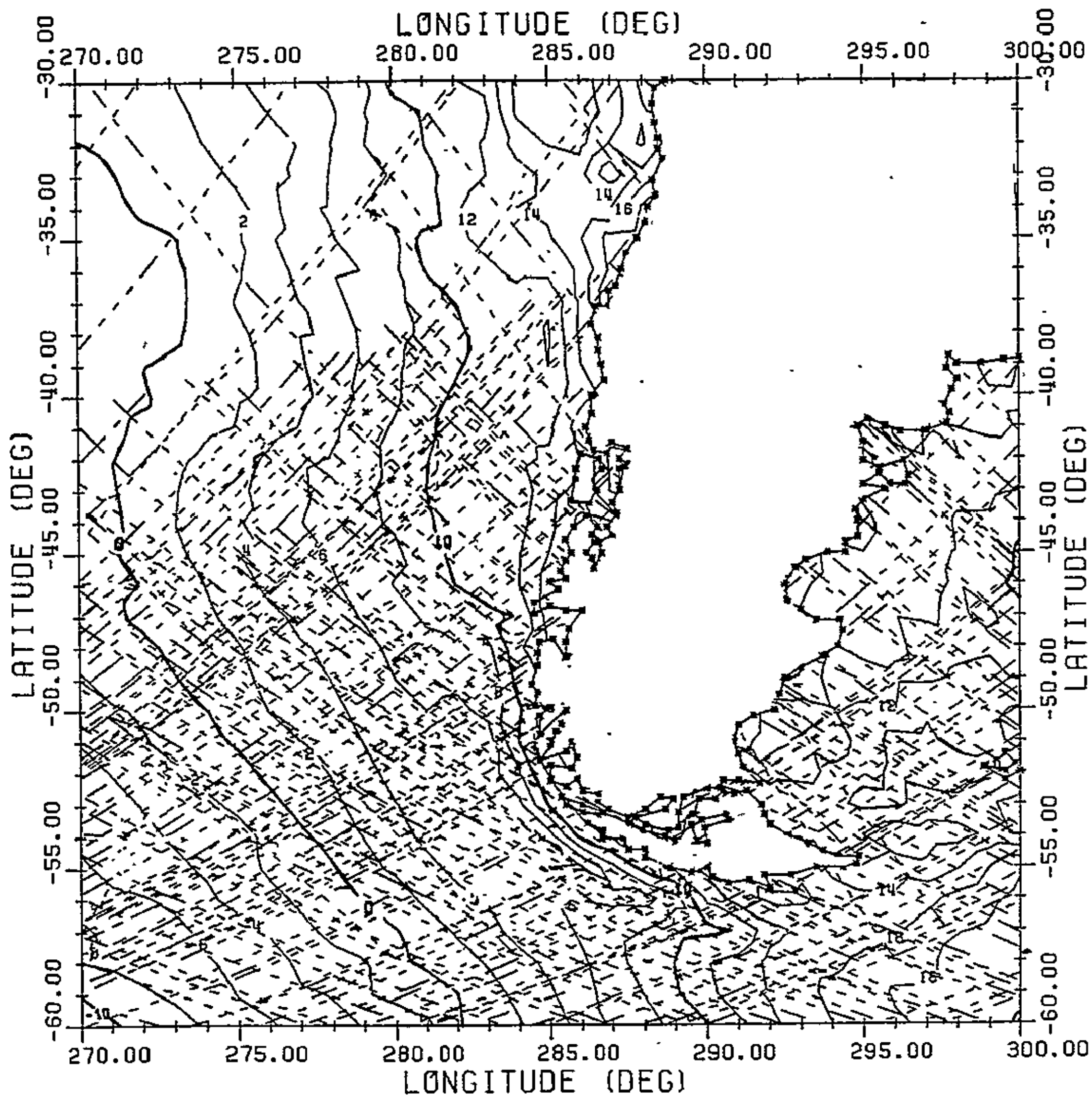

Figure 41

Precision of Prediction - South America

Grid Interval 1°
Contour Interval 0.5 m
Scale 1: 500,000

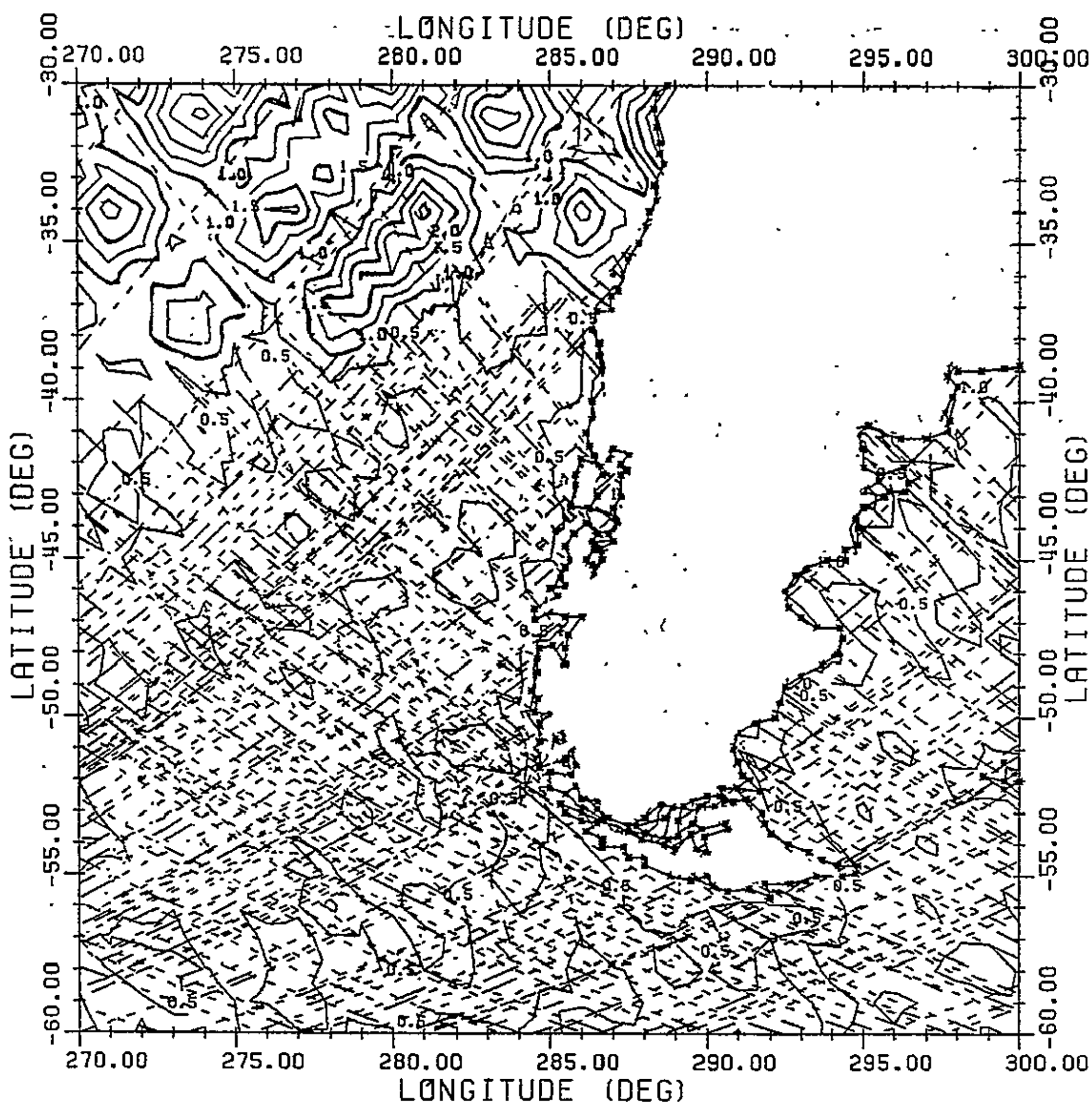

Figure 42

Geoidal Undulations - N. E. Pacific

Grid Interval 1° x 1°
Contour Interval 2 m
Scale 1: 500,000

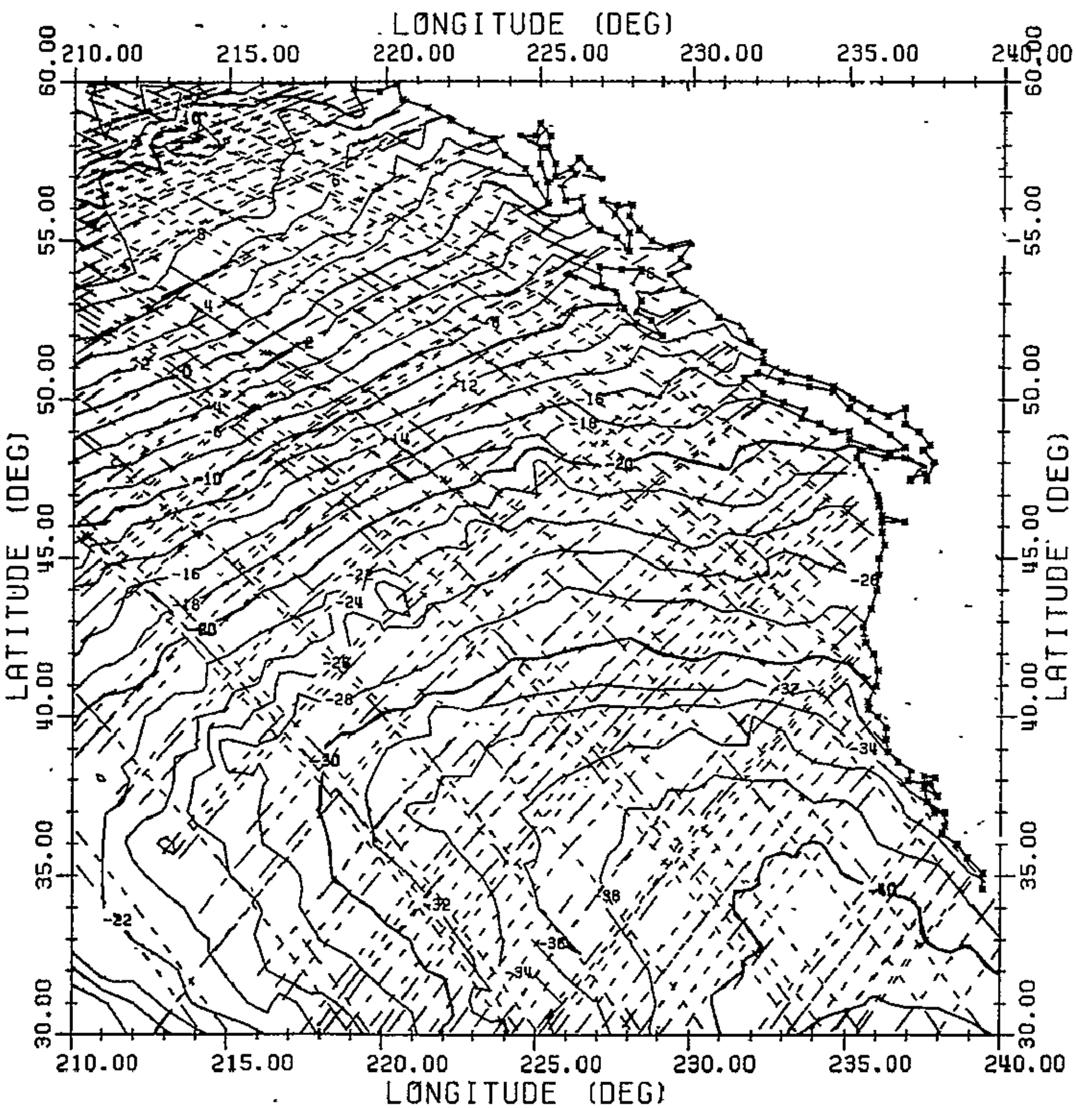

Figure 43

Precision of Prediction - N. E. Pacific

Grid Interval 1° x 1°
Contour Interval 0.5 m
Scale 1: 500,000

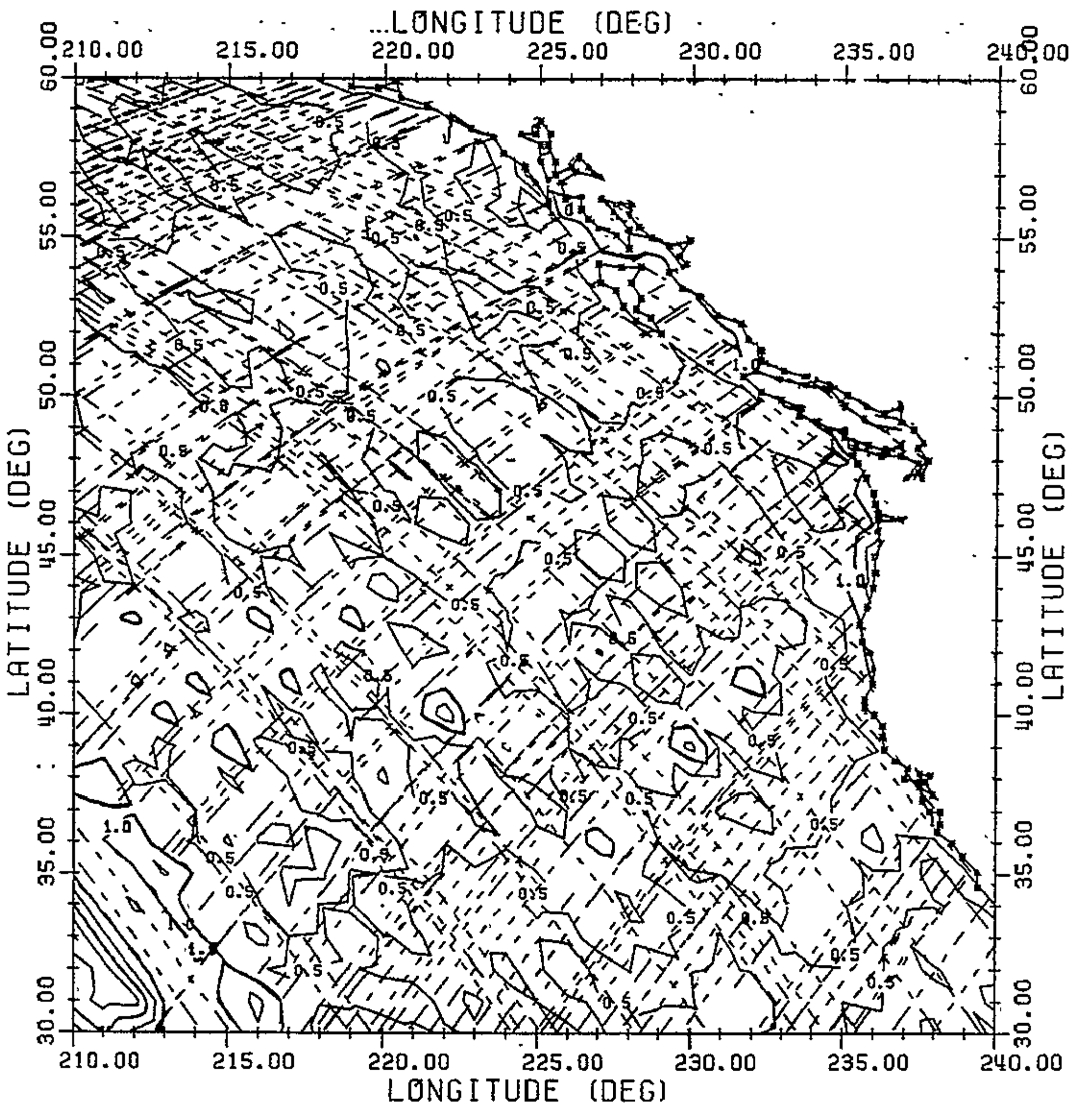

ORIGINAL PAGE IS
OF POOR QUALITY

Figure 44

Geoidal Undulations - N. E. Pacific

Grid Interval 1° x 1°
Contour Interval 2 m
Scale 1: 500,000

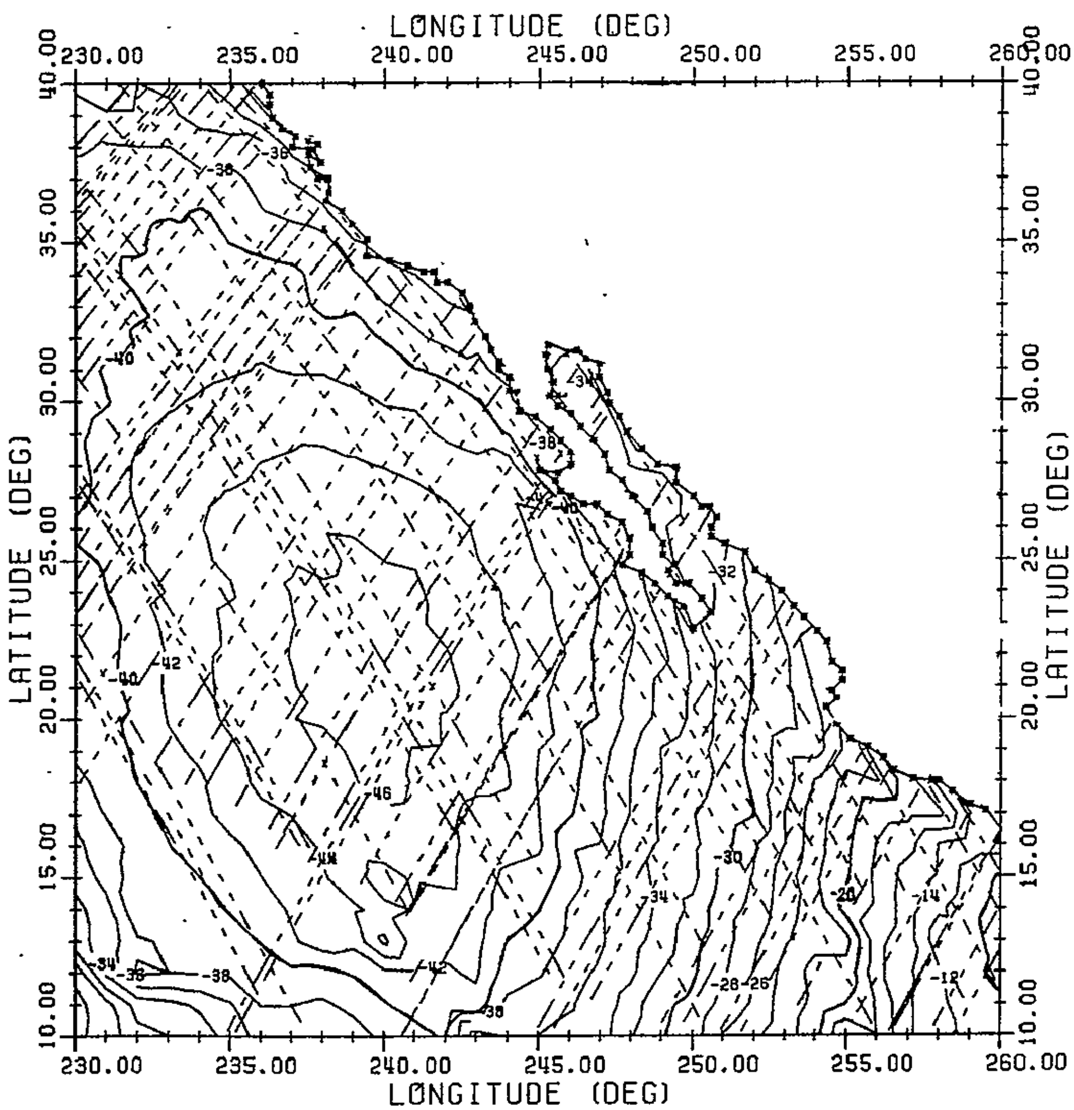

Figure 45

Precision of Prediction - N. E. Pacific

Grid Interval 1° x 1°
Contour Interval 0.5 m
Scale 1: 500,000

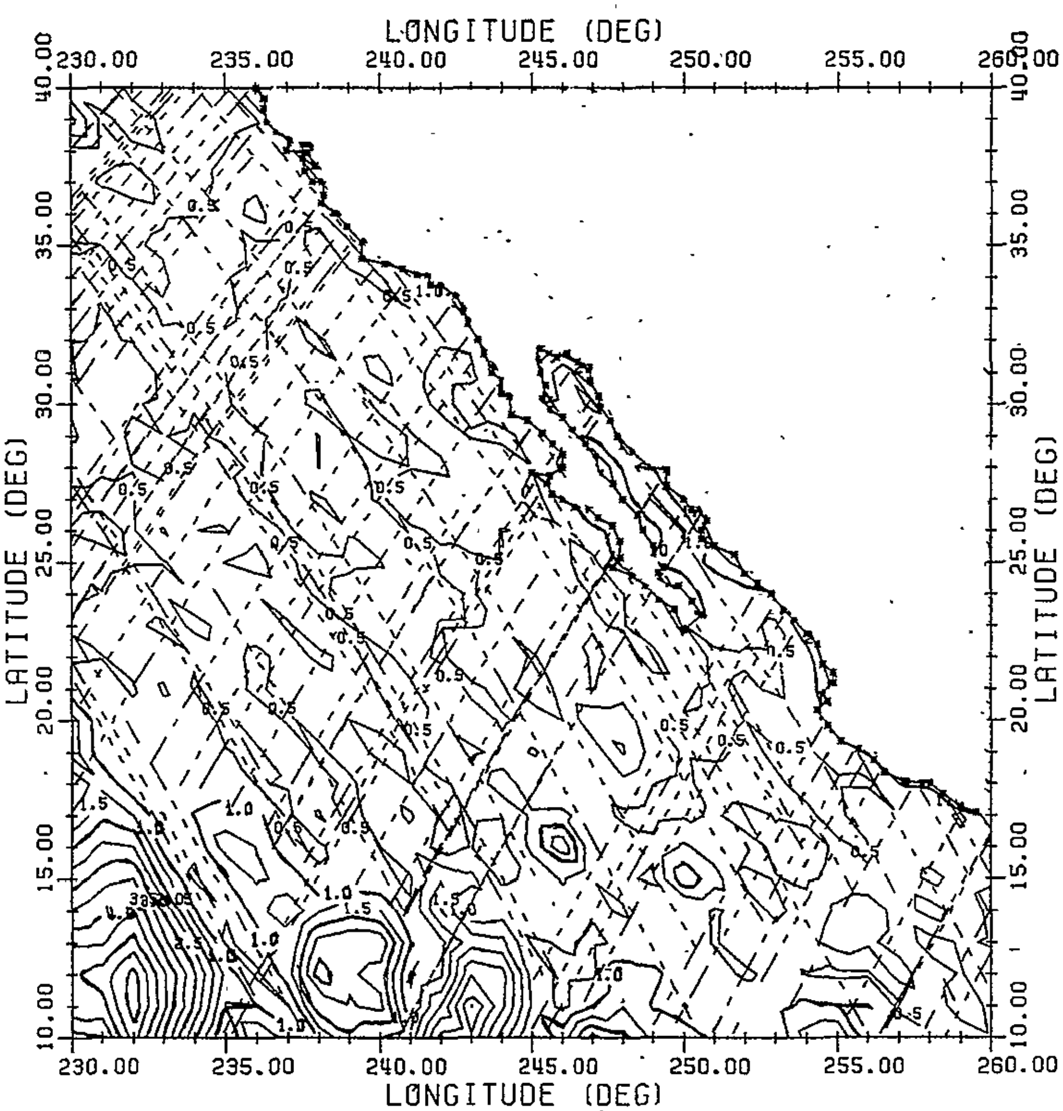

6. Conclusions

It is apparent from the foregoing that it is possible to obtain values of the geoidal undulation (or its approximation) from GEOS-3 altimetry with an accuracy which is of the order of ± 0.5 m to ± 1.0 m. It is difficult to ascertain an exact accuracy for this parameter as the geoids used for comparison themselves have uncertainties which are of this same order of magnitude.

It also appears that contouring the geoid over the ocean based on undulations predicted at 1° intervals produces maps which are representative of the geoid. The contour lines are expected to have an accuracy of ± 1 m, assuming the grid values themselves are error free. The precision of prediction for each geoid map is shown graphically in an associated map, and it would be possible to obtain some estimate of the absolute accuracy of the contour lines by combining the variance of the prediction with the variance of contouring. In areas well covered with altimetry data, and this is the case in most areas included in this report, the contouring error is theoretically estimated to be ± 1.2 m.

The altimetry data contains signals of higher frequency than the 1° half wave-length frequency inferred by the grid spacing. Areas with high frequency features such as the Philippines Trench or the Tonga Trench would benefit by use of a smaller grid interval, perhaps as small as the $0.^\circ 3$ which approximates the spacing of the altimeter data.

Discrepancies between orbits at crossover points have not (apparently) produced any problems in the contouring procedure. It is probable that the 2 m contour interval is too coarse to show any effect which may be produced by these discrepancies.

In summary, the contouring program produces reliable regional geoid maps from the GEOS-3 altimetry data. It is expected that, as more data becomes available in areas at present poorly covered, the mapping program will continue until all ocean areas of the world will be covered by the standard $30^\circ \times 30^\circ$ geoid maps.

Bibliography

Davis, John C., Statistics and Data Analysis in Geology, John Wiley and Sons, Inc., New York, 1973.

Jordan, Stanley K., "Self-Consistent Models for the Gravity Anomaly Vertical Deflections and Undulation of the Geoid", Journal of Geophysical Research, Vol. 77, No. 2.

Lachapelle, Gérard, Physical Geodesy at the Geodetic Survey, Geodetic Survey of Canada, Ottawa, October, 1976.

Marsh, J. and E. Chang, 5' Detailed Gravimetric Geoid in the Northwestern Atlantic Ocean, NASA Goddard Space Flight Center, Greenbelt, Maryland, December, 1976.

Moritz, Helmut, Advanced Least Squares Methods, Department of Geodetic Science Report No. 175, The Ohio State University, Columbus, 1972.

Pearson II, Frederick, Map Projection Equations, Naval Surface Weapons Center, Dahlgren, Virginia, NSWC/DL TR-3624, 1977.

Rapp, Richard H., Incomplete Final Results for Sea Surface Topography and Gravity Anomalies from GEOS-3 Altimeter Data, Department of Geodetic Science, The Ohio State University, Columbus, November, 1977.

Richardus, P., "The Precision of Contour Lines and Contour Maps of Large and Medium Scale Maps", Photogrammetria, Vol. 29, 1973.

Rummel, Reiner, GEOS-3 Altimeter Data Processing for Gravity Anomaly Recovery, Department of Geodetic Science, The Ohio State University, Columbus, 1976.

Sjöberg, Lars, Test of a Kalman Model and a Deterministic Model for Prediction of Gravity Anomalies, Report of the Royal Institute of Technology, Division of Geodesy, Stockholm, 1975.

Snowden, John M., A Fortran IV Program for the Graphical Representation of Gravity Anomaly Data, Department of Geodetic Science Report No. 123, The Ohio State University, Columbus, 1969.

Tscherning, C. C. and Rapp, R. H., Closed Covariance Expressions for Gravity Anomalies, Geoid Undulations, and Deflections of the Vertical Implied by Anomaly Degree Variance Models, Department of Geodetic Science Report No. 208, The Ohio State University, Columbus, 1974.

Wagner, C. A., The Spectrum of the Geoid from Altimeter Data, NASA Goddard Space Flight Center, Document TM-X-71337, X-921-77-63, Greenbelt, Maryland, 1977.

Appendix A

Use of the Contouring Program

A.1. Data Input

The altimetry data is read directly from the relevant tape which, in the case of the areas mapped in this report, is either GS 102 or GS 110.

Card 1. Format: 5F10.2, 3I5, F5.1, 2I5

(i) PHI1, PHI2, LAM1, LAM2. (REAL*4) Units - decimal degrees.

Sets the upper and lower limits in latitude and longitude for the map. Also defines the limits of the inner window. Maximum number of points currently acceptable is 7,000.

(ii) OVLAP (REAL*4) Units - decimal degrees

Sets the margin beyond the plotting limits in (1) from which data will be read (i. e. the outer window). This is to ensure adequate data is available for the prediction of grid values on the map borders.

(iii) NY, NX (INTEGER)

Denotes the number of grid intervals in the North-South and East-West directions (respectively). Values which produce a 1° grid spacing appear to be optimum for areas well covered by altimetry data.

Note: The arrays X, Y, Z and SD must be dimensioned NY + 1, NX + 1 in the main program and in subroutines AXPLT and PRDT.

(iv) IAO (INTEGER)

If IAO = n, every n th point within the inner windown will be plotted and identified.
If IAO = 0, neither points nor tracks will be plotted.
If IAO > 7000, the tracks will be plotted in dashed lines, but no points will be plotted.

(v) AXLAB (REAL*A) Decimal degrees

Spacing for labelling of axes. For example, if AXLAB = 5.0, a tick and a latitude or longitude value will be printed every 5 degrees.

(vi) IND (INTEGER)

This enables selection of the projection for the plot (see Program MAIN for details).

(vii) IND1 (INTEGER)

Shoreline plot indicator. If IND1 = 0, shoreline will not be plotted. If IND1 > 0, shoreline will be plotted.

Card 2. Unformatted

(i) SCFAC (REAL*4)

Scale factor applied to the plot to reduce it to appropriate dimensions. This will depend on the extent of the plot (note (i), Card 1), the chosen projection and the desired size of the plot. If the scale chosen is, for example, 1/250000 then SCFAC = 250000.0.

(ii) CNTINT (REAL*4)

Contour interval in meters. This should be at least twice the expected accuracy of the data.

(iii) NLC, NDL, HCL, SL, KSM and WTCP. Refer to subroutine CGTOUR.

A. 2. Output

(i) The program prints out the details read on cards 1 and 2. It also lists in inches the limits of the plot, and the increments of the grid in N-S and E-W directions.

(ii) The data accepted for use in the prediction (i.e. data accepted into the outer window) is now listed. The sequence of the listing is: (i) sequence number within window, (ii) observation identifying number, (iii) latitude and (iv) longitude in decimal degrees, (v) undulation value, (vi) easting and (vii) northing of point at plotting scale in decimal inches and (viii) a flag, indicating if the point is the first of a section within an orbit.

(iii) The initial and final points used to plot segments of the tracks is now listed.

(iv) Details of data selected for the prediction of each grid point is listed row by row, row 1 being the row of least latitude.

(v) The predicted values of the undulation and the error of prediction are now summarized in table form for convenience.

(vi) Finally, the details of data used for plotting the axes are now listed.

A.3. Check List When Using the Contouring Program

Check

(i) 2nd last data card to certify (a) Map Limits, (b) No. of Grid Intervals in Y and X, (c) Track Plot Indicator IAO and (d) Projection choice are correct.

(ii) DIMENSIONS of X, Y, Z and SD in MAIN program and subroutines PRDT and AXPLT. The dimensions of these arrays should be NY + 1, NX + 1.

(iii) DATA card in MAIN program; INC should be set so that no. of data allowed into outer window does not exceed 7,000. Note if INC = n, only every n th point in window is used.

(iv) Tape and Tape File Numbers are correct for the area to be mapped.

Appendix B: Flow Chart - Main Program

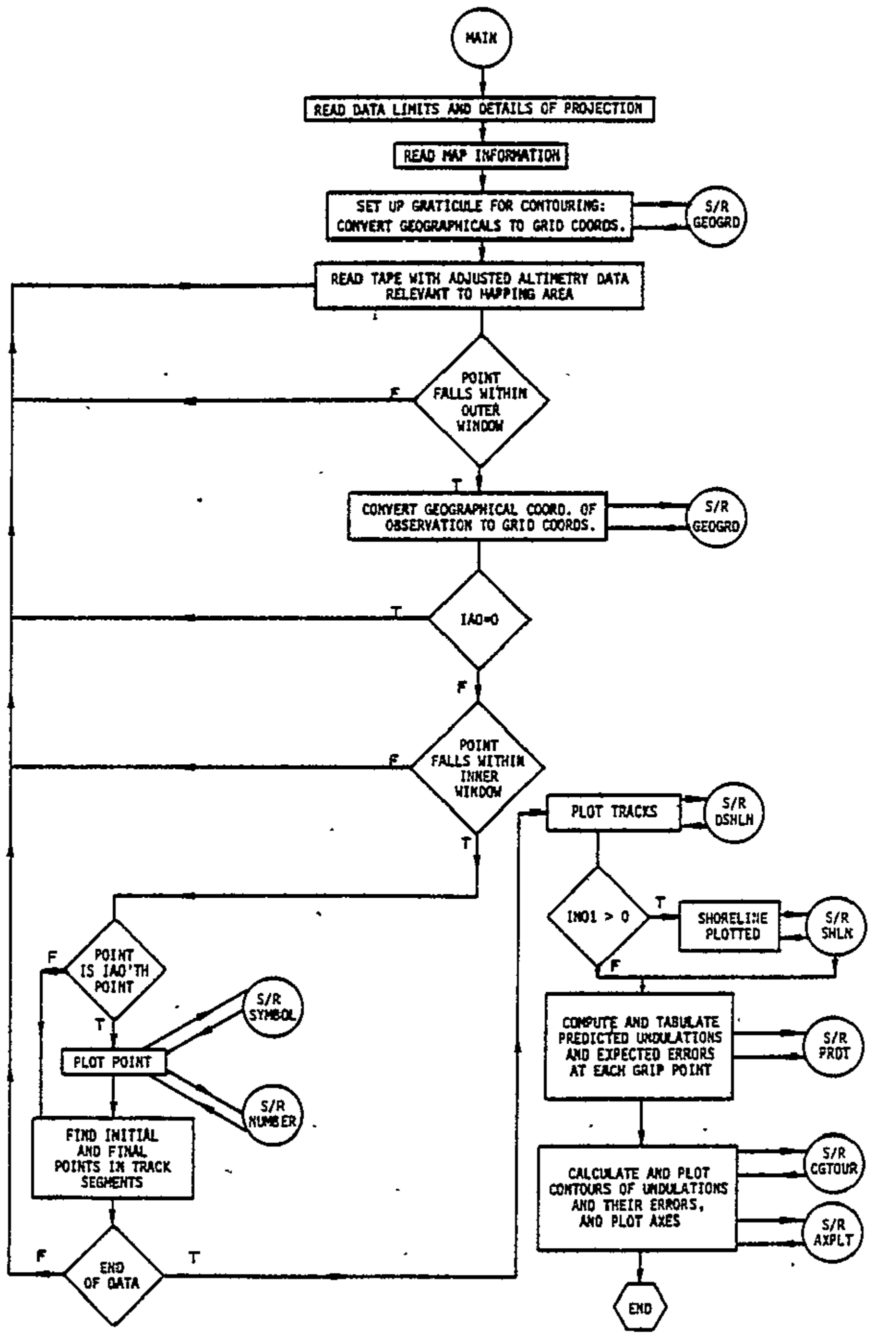

1. Report No
NASA CR-141439

2. Government Accession No.

3. Recipient's Catalog No.

4. Title and Subtitle
The Prediction and Mapping of Geoidal Undulations from GEOS-3 Altimetry

5. Report Date
April 1978

6. Performing Organization Code

7. Author(s)
William Kearsley

8. Performing Organization Report No.

9. Performing Organization Name and Address
The Ohio State University
Research Foundation
Columbus, OH 43212

10. Work Unit No.

11. Contract or Grant No.
NAS6-2484

12. Sponsoring Agency Name and Address
National Aeronautics and Space Administration
Wallops Flight Center
Wallops Island, VA 23337

13. Type of Report and Period Covered
Contractor Report

14. Sponsoring Agency Code

15. Supplementary Notes

16. Abstract

From the adjusted altimeter data, one gets an approximation to the geoid height in ocean areas. This paper describes methods developed in the Department of Geodetic Science to produce 'geoid' maps in these areas. Geoid heights are obtained for grid points in the region to be mapped, and two of the parameters critical to the production of an accurate map are investigated. These are (i) the spacing of the grid, which must be related to the half-wavelength of the altimeter signal whose amplitude is the desired accuracy of the contour, and (ii) the method adopted to predict the grid values.

In the final production program, least squares collocation was used to find geoid undulations on a 1° grid in the mapping area. Twenty maps, with their associated precisions, have been produced and are included in this report. These maps cover the Indian Ocean, Southwestern and Northeastern portions of the Pacific Ocean, and Southwest Atlantic and the U.S. Calibration Area. Lack of data has precluded further mapping at this stage.

17. Key Words (Suggested by Author(s))
GEOS-3
geoid
gravity anomaly

18. Distribution Statement
Unclassified - unlimited

STAR Category - 42,46,48

19. Security Classif. (of this report)	20. Security Classif. (of this page)	21. No. of Pages	22. Price*
Unclassified	Unclassified	72	

*For sale by the National Technical Information Service, Springfield, Virginia 22151